

Low-Energy Measurements of the Weak Mixing Angle

K.S. KUMAR

Department of Physics, University of Massachusetts, Amherst, MA 01003

email: kkumar@physics.umass.edu

SONNY MANTRY

Northwestern University and Argonne National Laboratory

W.J. MARCIANO

Brookhaven National Laboratory

P.A. SOUDER

Syracuse University

Key Words Weak Neutral Currents, Weak Mixing Angle, Precision Tests of
the Standard Model, Electroweak Radiative Corrections

Abstract

We review the status of precision measurements of weak neutral current interactions, mediated

by the Z^0 boson, at $Q^2 \ll M_Z^2$. They can be used to extract values for the weak mixing angle $\sin^2 \theta_W$, a fundamental parameter of the $SU(2)_L \times U(1)_Y$ electroweak sector of the Standard Model. Apart from providing a comprehensive test of the electroweak theory at the quantum loop level, such measurements allow indirect access to new physics effects at and beyond the TeV scale. After a theoretical introduction and a brief overview of the three most precise low Q^2 weak mixing angle determinations, we describe the ongoing experimental program and prospects for future more sensitive studies. We also compare sensitivities of planned and proposed measurements to physics beyond the Standard Model.

CONTENTS

| | |
|--|----|
| INTRODUCTION | 3 |
| <i>Historical Context</i> | 3 |
| <i>The Weak Mixing Angle and Quantum Corrections</i> | 6 |
| <i>The Weak Mixing Angle at $Q^2 \ll M_Z^2$</i> | 10 |
| PAST MEASUREMENTS | 12 |
| <i>Atomic Parity Violation in Cesium</i> | 13 |
| <i>SLAC E158</i> | 14 |
| <i>NuTeV</i> | 16 |
| PARITY-VIOLATING ELECTRON SCATTERING | 18 |
| <i>Qweak</i> | 19 |
| <i>MOLLER</i> | 20 |
| <i>Deep Inelastic Scattering at 6 GeV</i> | 22 |
| <i>SOLID</i> | 22 |
| <i>P2</i> | 24 |
| SENSITIVITY TO PHYSICS BEYOND THE STANDARD MODEL | 25 |
| <i>New Contact Interactions</i> | 25 |
| <i>New Heavy Z' Bosons</i> | 28 |
| <i>Dark Parity Violation</i> | 30 |

| | |
|--|----|
| <i>Weak Charges and New Physics</i> | 31 |
| SELECTED THEORETICAL ISSUES | 34 |
| <i>Radiative Corrections to Parity-Violating Møller Scattering</i> | 34 |
| <i>Running of the Weak Mixing Angle</i> | 36 |
| <i>Weak Charge of the Proton</i> | 39 |
| OTHER POTENTIAL FUTURE MEASUREMENTS | 43 |
| <i>Atomic Parity Violation</i> | 43 |
| <i>Neutrino Scattering</i> | 44 |
| <i>Parity Violating Electron Scattering off ¹²C</i> | 44 |
| <i>Weak Mixing Angle at an Electron-Ion Collider</i> | 46 |
| SUMMARY AND OUTLOOK | 47 |

1 INTRODUCTION

1.1 Historical Context

In 1961, Sheldon Glashow (1) introduced an $SU(2)_L \times U(1)_Y$ symmetry that would form the basis for electroweak unification. In modern terminology, it contained four spin-1 vector bosons W_μ^+ , W_μ^0 , W_μ^- and B_μ^0 along with two independent couplings, g and g' . Mixing gave rise to a massless photon and its orthogonal massive partner now known as the Z^0 boson:

$$\begin{aligned}
 A_\mu &= B_\mu^0 \cos \theta_W + W_\mu^0 \sin \theta_W \\
 Z_\mu &= W_\mu^0 \cos \theta_W - B_\mu^0 \sin \theta_W.
 \end{aligned}
 \tag{1}$$

That formalism marked the birth of the weak mixing angle, θ_W , defined by $\tan \theta_W = g'/g$ or in terms of the electromagnetic coupling $e = gg'/\sqrt{g^2 + g'^2}$: $\sin \theta_W = e/g$. Particle masses were arbitrarily put in by hand and were unre-

lated to other parameters in the theory.

In 1967, Steven Weinberg (2) appended the Higgs mechanism (3, 4, 5, 6, 7) to $SU(2)_L \times U(1)_Y$ electroweak gauge unification via a complex, spin-0 scalar doublet whose vacuum expectation value spontaneously broke the gauge symmetry to $U(1)_{em}$ and gave rise to W^\pm and Z^0 masses related by $m_W = m_Z \cos \theta_W$. It also led to a physical spin-0 Higgs boson with arbitrary mass, m_H . As an added bonus, the Higgs which originally accommodated charged lepton masses, later proved well-suited to include quark masses and mixing (8), including CP violation. Weinberg speculated that the theory might be renormalizable and that weak neutral current effects, mediated by the Z^0 boson, should be observed in neutrino scattering.

In 1971, Gerhard 't Hooft (9) proved renormalizability for gauge theories with spontaneous symmetry breaking and weak neutral currents were discovered in 1973 (10). Together, they confirmed the consistency and basic ingredients of electroweak unification.

The combination, $SU(2)_L \times U(1)_Y$ gauge invariance + Higgs doublet + renormalizability led to natural relationships among the bare (unrenormalized) gauge boson masses and couplings (11)

$$\sin^2 \theta_W^0 = e_0^2/g_0^2 = 1 - m_W^0/m_Z^0. \quad (2)$$

Those relations are respected by the renormalized parameters, up to finite calculable radiative corrections (11, 12). Such corrections, discussed in Sec. 1.2, test the theory at its quantum loop level and probe for potential “new physics” effects.

By the mid-1970s, the basic features of $SU(2)_L \times U(1)_Y$ electroweak unification were nearly established. The quark model (including charm) and its associated strong $SU(3)_c$ color gauge interactions, quantum chromodynamics (QCD), were

elegantly incorporated while weak neutral current effects continued to be observed at about the predicted rate. However, it was not clear that the model's specific weak neutral current interaction (2)

$$\frac{g}{\cos \theta_W} Z_\mu \bar{f} \gamma^\mu (T_{3f} - 2Q_f \sin^2 \theta_W - T_{3f} \gamma_5) f, \quad T_{3f} = \pm 1/2 \quad (3)$$

was correct. In particular, that interaction implied a small degree of parity violation throughout low energy physics due to $\gamma - Z^0$ interference. Such effects were enhanced in atoms with a large number of protons (Z) and neutrons (N) by the coherent weak charge that quantifies the Z^0 -nucleus vector coupling (13)

$$Q_W(Z, N) = Z(1 - 4 \sin^2 \theta_W) - N. \quad (4)$$

Unfortunately, the early efforts to measure atomic parity violation (APV) using ^{209}Bi failed to observe the expected effect (14, 15) and cast some doubt on the specific form of Eqn. (3). (Later studies with ^{209}Bi , ^{205}Tl and ^{133}Cs observed parity violation at the expected level (16, 17, 18, 19)).

In 1978, the now classic E122 experiment at SLAC, led by Charles Prescott searched for a helicity dependence in the inclusive cross-section $\sigma_{R(L)}$ for deep-inelastic scattering of longitudinal polarized electrons off unpolarized ^2H (20). Defining a parity-violating asymmetry

$$A_{PV} \equiv \frac{\sigma_R - \sigma_L}{\sigma_R + \sigma_L}, \quad (5)$$

the measured value, $A_{PV} \simeq 1.5 \times 10^{-4}$, confirmed the predicted form in Eqn. (3) and determined $\sin^2 \theta_W$ with relatively good precision ($\pm 10\%$): $\sin^2 \theta_W \simeq 0.22(2)$.

That milestone experiment established $\text{SU}(3)_C \times \text{SU}(2)_L \times \text{U}(1)_Y$ as the Standard Model (SM). In addition, the measured value of $\sin^2 \theta_W$ lent support to grand unified theories (GUTS) (21, 22) such as $\text{SU}(5)$, $\text{SO}(10)$, ... Assuming

a “great desert” *i.e.* no “new physics” between the SM and unification scale $m_X \simeq 10^{15}$ GeV, those theories predicted at one loop ($\alpha = e^2/4\pi \simeq 1/137$) (23)

$$\sin^2 \theta_W \approx \frac{3}{8} \left[1 - \frac{109\alpha}{18\pi} \ln \frac{m_X}{m_W} \right] \simeq 0.21 \quad (\text{One loop minimal SU(5)}) \quad (6)$$

in accord with the SLAC E122 value. (That simplistic scheme was, however, later ruled out by its failure to accommodate complete coupling unification and proton decay ($p \rightarrow e^+ \pi^0$) constraints. Nevertheless, GUTS continue to be an interesting paradigm; still used to advance low energy supersymmetry (24) as a unifying desert ingredient.)

1.2 The Weak Mixing Angle and Quantum Corrections

In the 1980s, it became clear that in order to rigorously test the SM and GUTS at the level of their quantum corrections, $\sin^2 \theta_W$ as well as the other electroweak parameters in Eqn. (2) (m_W , m_Z , α and $G_F = g^2/4\sqrt{2}m_W^2$) would have to be determined with very high precision (25, 26), $\mathcal{O}(\pm 0.1\%)$ or better. Some were already known orders of magnitude better than needed; currently (27, 28) $\alpha^{-1} = 137.035999173(35)$ and $G_F = 1.1663787(6) \times 10^{-5}$ GeV⁻². In the case of vector boson masses, great progress was later made at LEP and the Tevatron (29): $m_Z = 91.1876(21)$ GeV and $m_W = 80.385(15)$ GeV.

For $\sin^2 \theta_W$, an important issue was the requirement of a rigorous definition of the renormalized weak mixing angle for precision experimental extraction. At first, the on-shell definition (30, 31)

$$\sin^2 \theta_W \equiv 1 - m_W^2/m_Z^2 \quad (7)$$

proved popular. However, after the top quark mass was found to be large (currently accepted value is $m_t = 173.3(8)$ GeV), the on-shell definition was largely

abandoned, because its use induced large misleading $\mathcal{O}(\alpha m_t^2/m_W^2)$ radiative corrections to weak neutral current processes. Instead, at LEP, it became practice to employ an effective $\sin^2 \theta_W^{eff}$ defined by the $Z^0 \mu^+ \mu^-$ coupling at the Z^0 pole. The only drawback was the complexity of finite renormalized counterterms required for non- Z^0 pole applications.

For computational convenience and comparison with GUT predictions, it was easier to employ the more theoretically motivated (but unphysical) $\overline{\text{MS}}$ (modified minimal subtraction) prescription (originally introduced for QCD) (25, 32)

$$\sin^2 \theta_W(\mu)_{\overline{\text{MS}}} = e^2(\mu)_{\overline{\text{MS}}}/g^2(\mu)_{\overline{\text{MS}}} \quad (8)$$

with an arbitrary sliding mass scale μ . Numerically, it is related to $\sin^2 \theta_W^{eff}$ used at LEP by (33)

$$\sin^2 \theta_W(m_Z)_{\overline{\text{MS}}} = \sin^2 \theta_W^{eff} - 0.00028 \quad (9)$$

making translation between the two schemes straightforward.

Currently, the two best determinations of $\sin^2 \theta_W(m_Z)_{\overline{\text{MS}}}$ come from the right-left Z pole production asymmetry A_{RL} at SLAC (34)

$$\sin^2 \theta_W(m_Z)_{\overline{\text{MS}}} = 0.23070(26) \quad A_{RL} \quad (10)$$

and the $Z \rightarrow b\bar{b}$ forward-backward asymmetry $A_{FB}(b\bar{b})$ measured at LEP1 (35)

$$\sin^2 \theta_W(m_Z)_{\overline{\text{MS}}} = 0.23193(29). \quad A_{FB}(b\bar{b}) \quad (11)$$

Unfortunately, they disagree by 3.2 sigma. Even the overall LEP1 average including lepton forward-backward asymmetries and τ polarization, $\sin^2 \theta_W(m_Z)_{\overline{\text{MS}}} = 0.23161(21)$, is somewhat high compared to Eqn. (10). Nevertheless, all Z^0 pole measurements are usually averaged to give

$$\sin^2 \theta_W(m_Z)_{\overline{\text{MS}}} = 0.23125(16) \quad Z \text{ pole Ave.} \quad (12)$$

for comparison with other precision studies. The spread in the most precisely measured values of $\sin^2 \theta_W(m_Z)_{\overline{\text{MS}}}$ remains, however, somewhat troubling and needs to be resolved, as underscored by an example of their different implications discussed toward the end of this subsection.

The exquisite precision achieved in the measurements of m_Z , m_W and $\sin^2 \theta_W$ allows for important tests of the electroweak theory at the level of quantum loops. In the process of renormalization, finite radiative corrections upset the natural relations of Eqn. 2. The fractional deviation has been historically (30, 31) called Δr , and is primarily due to fermion and boson vacuum polarizations (including those involving top quarks and SM bosons that are heavier than the energy scales of various measurements), but could also receive contributions from other indirect effects of even higher mass scale “new physics”. Conventionally, three different quantities have been used to parametrize the deviations in the finite radiative corrections from zero (30, 31, 36, 37, 38, 39), because of their distinctly different dependencies on m_t , m_H and “new physics”:

$$(\Delta r)^{\text{expt}} = 1 - [\pi\alpha/\{\sqrt{2}G_F m_W^2(1 - m_W^2/m_Z^2)\}] = 0.0350(9) \quad (13)$$

$$(\Delta r)^{\text{SM}} = 0.0364(3) + 3.4 \times 10^{-3} \ln [m_H/126 \text{ GeV}]$$

$$(\Delta \hat{r})^{\text{expt}} = 1 - [2\sqrt{2}\pi\alpha/\{G_F m_Z^2 \sin^2 2\theta_W(m_Z)_{\overline{\text{MS}}}\}] = 0.0598(5) \quad (14)$$

$$(\Delta \hat{r})^{\text{SM}} = 0.0598(2) + 1.4 \times 10^{-3} \ln [m_H/126 \text{ GeV}]$$

$$(\Delta r_{\overline{\text{MS}}})^{\text{expt}} = 1 - [\pi\alpha/\{\sqrt{2}G_F m_W^2 \sin^2 \theta_W(m_Z)_{\overline{\text{MS}}}\}] = 0.0699(7)(4)$$

$$(\Delta r_{\overline{\text{MS}}})^{\text{SM}} = 0.0693(2) + 6.5 \times 10^{-4} \ln [m_H/126 \text{ GeV}] \quad (15)$$

where the dependence of the first two corrections on m_H provide sensitivity to it, while $\Delta r_{\overline{\text{MS}}}$ has less dependence on m_H . We emphasize that the values on the right (on the first line of each equation) are purely experimental determinations.

Those on the second line of each equation incorporate detailed calculations of SM loop corrections (37, 38, 39, 40, 41) (assuming no “new physics”) and using experimental measurements of α_{EM} , G_F , m_Z and m_t as input. The theoretical predictions are dominated by a +7% shift due to fermion vacuum polarization effects that lead to the running of α_{EM} from $\alpha(0) = 1/137$ to $\alpha(m_Z)_{\overline{\text{MS}}} = 1/127.9$, but also include important dependences on m_H and m_t . Note also, that we have normalized the predictions at $m_H = 126$ GeV, the tentative value of the new scalar resonance recently discovered at the Large Hadron Collider (42, 43).

Alternatively, one can obtain, from the first two corrections the predictions (Eqns. 13–14): $m_W = 80.362(6)$ GeV and $\sin^2 \theta_W(m_Z)_{\overline{\text{MS}}} = 0.23124(6)$ for $m_H = 126$ GeV, where the uncertainties are due to the errors in m_t and hadronic effects. (The errors are approximately doubled if one includes estimated uncertainties in uncalculated higher order effects (44)). The agreement between those predictions and the corresponding world averages of current measurements constitutes a beautiful verification of the electroweak theory at the quantum loop level and constrains many “new physics” scenarios. If instead, one takes the world averages for m_W and $\sin^2 \theta_W$, one obtains $m_H = 97_{-20}^{+24}$ GeV in relatively good accord with the LHC finding but somewhat low, still leaving some room for “new physics”.

The experimental determinations of m_W and $\sin^2 \theta_W$ also provide a direct probe of “new physics” by testing the validity of the third $\Delta r_{\overline{\text{MS}}}$ relation (Eqn. 15). For example, taking $m_H \simeq 126$ GeV but allowing for N_D heavy new chiral doublets ($N_D = 4$ for a fourth generation) via $S = N_D/6\pi$ or a heavy $W^{*\pm}$ excited W boson leads, upon comparing with experiment, to (45, 46)

$$\Delta r_{\overline{\text{MS}}}(m_Z) = 0.0693(2) + 0.0085S + \left(\frac{m_W}{m_{W^*}}\right)^2 = 0.0699(8) \quad (16)$$

or

$$\begin{aligned}
 S = 0.07(9) &\rightarrow N_D \leq 4 && \text{(One – sided 95\%CL),} \\
 m_{W^*} &> 2.2 \text{ TeV} && \text{(One – sided 95\%CL).} \tag{17}
 \end{aligned}$$

Such constraints appear to tightly restrict “new physics”. However, they are quite dependent on the Z^0 pole average $\sin^2 \theta_W(m_Z)_{\overline{\text{MS}}}$ employed as well as the overall error. If one instead uses the $A_{fB}(b\bar{b})$ value in Eqn. 11, it suggests $S \sim 0.4$ or $N_D \simeq 6-7$, more in keeping with dynamical symmetry breaking (technicolor) or 4th generation scenarios. Additionally, in Eqn. 15, the larger(smaller) error is due to the uncertainty in $\sin^2 \theta_W(m_W)$. This underscores the need for improved experimental determinations of $\sin^2 \theta_W$, the topic of this review.

1.3 The Weak Mixing Angle at $Q^2 \ll M_Z^2$

What do low energy determinations of $\sin^2 \theta_W$, the subject of this review, add to the above discussion? How do they complement the already precise Z^0 pole measurements? Currently, there are 3 low Q^2 measurements of $\sin^2 \theta_W$ at the $\pm 1\%$ level or better. They will be reviewed in Sec. 2, including details and caveats associated with each extraction. Here, we summarize the results extrapolated to m_Z scale for comparison with Z^0 pole measurements (47, 48, 49)

$$\sin^2 \theta_W(m_Z)_{\overline{\text{MS}}} = 0.2283(20) \quad \text{Cs APV at } \langle Q \rangle \simeq 2.4 \text{ MeV} \tag{18}$$

$$\sin^2 \theta_W(m_Z)_{\overline{\text{MS}}} = 0.2329(13) \quad \text{Møller } A_{PV} \text{ at } \langle Q \rangle \simeq 160 \text{ MeV} \tag{19}$$

$$\sin^2 \theta_W(m_Z)_{\overline{\text{MS}}} = 0.2356(16) \quad \nu_\mu N \text{ at } \langle Q \rangle \simeq 5 \text{ GeV} \tag{20}$$

Those values are not directly competitive with Z^0 pole results. Even the average of Eqns. 18–20: $\sin^2 \theta_W(m_Z)_{\overline{\text{MS}}} = 0.2328(9)$ *i.e.* $\mathcal{O}(\pm 0.4\%)$ lends little to the above discussion. However, as we discuss in Sec. 3, future polarized electron

scattering asymmetries at low Q^2 are expected to reach similar precision to the best Z^0 pole measurements: $\mathcal{O}(\pm 0.1 - 0.2\%)$. At that level, they may help resolve differences between the SLAC and LEP1 results, or perhaps, as we shall discuss, find interesting new effects.

Apart from improved precision testing of the electroweak theory at the quantum loop level, low Q^2 measurements are sensitive to classes of “new physics” effects to which Z^0 pole measurements are insensitive. The measurements in Eqns. 18–20 can already be used to constrain “new physics” such as Z' bosons or general 4-fermion contact interactions. Future more precise experiments are expected to probe the 1–20 TeV scale, as described in Sec. 4. We also show how such experiments may be used to explore very weakly coupled low mass scale “dark boson” effects.

In addition, the low Q^2 results already test the SM predicted running (25, 26, 32, 50, 51, 52) of $\sin^2 \theta_W$ as a function of Q^2 . The evolution of that quantity can be examined in the $\overline{\text{MS}}$ framework of Eqn. (8) using the $e(\mu)$ and $g(\mu)$ beta functions. The running is illustrated in Fig. 1 along with the three measurements with $\mu = \langle Q \rangle$ determined from each experiment’s average momentum conditions (53). The only drawback to that formalism is the unphysical $\overline{\text{MS}}$ discontinuities at $\mu = \langle Q \rangle =$ particle masses. To circumvent that feature, it is useful to define a more physical running weak angle (50, 51, 52, 54)

$$\sin^2 \theta_W(Q^2) = \kappa(Q^2) \sin^2 \theta_W(m_Z)_{\overline{\text{MS}}} \quad (21)$$

where $\kappa(Q^2)$ incorporates perturbative $\gamma - Z$ mixing through vacuum polarization and other smaller corrections. This is illustrated in Fig. 1 normalized such that $\kappa(Q^2 = m_Z^2) \simeq 1.000$ while $\kappa(0)$ turns out to be about 1.030. This 3% variation is particularly important for some low Q^2 polarized electron scattering asymmetries

proportional to $1 - 4 \sin^2 \theta_W(Q^2)$ (examples discussed in Sec. 3) that are very sensitive to small variations in $\sin^2 \theta_W(Q^2)$. Indeed, the 3% shift in $\sin^2 \theta_W$ results in a roughly 40% change in $1 - 4 \sin^2 \theta_W$, ($0.075 \rightarrow 0.046$ at $\langle Q \rangle \sim 0.1$ GeV).

Of course, to test the running of $\sin^2 \theta_W(Q^2)$ and try to unveil “new physics” requires confidence in the theoretical underpinnings of the various reactions studied. To that end, we examine in Sec. 5 the status of several theoretical issues, including hadronic uncertainties in $\kappa(0)$ and γZ^0 box diagrams. However, we emphasize that each experimental measurement should be compared with a calculation specific to the relevant experimental conditions including complete one-loop and leading two-loop effects and estimates of hadronic contribution uncertainties. The latter are under control for very low Q^2 and high Q^2 measurements but may require more careful studies at intermediate Q^2 . We conclude with a brief sketch of other potential ways to measure $\sin^2 \theta_W$ in Sec. 6, and provide a future perspective and outlook in Sec. 7.

2 PAST MEASUREMENTS

In the following section, we review the three most precise published measurements of $\sin^2 \theta_W$ at $Q^2 \ll M_Z^2$. The implications of the measurements for high and low scale dynamics will be addressed in Sec. 4. A comprehensive review of earlier experiments and associated developments can be found in Ref. (55); a very recent review addresses a broader class of weak neutral current observables (56).

2.1 Atomic Parity Violation in Cesium

One of the classic precision techniques in the field is the measurement of parity violation in atoms, as mentioned in Sec. 1. The electron-nucleus weak neutral current interaction mediated by Z^0 exchange can be characterized by a new term in the Hamiltonian with an overall strength $Q_W G_F$, where G_F is the Fermi constant and the weak charge Q_W was defined in Eqn. 4. The new interaction induces a parity-violating matrix element $Im(E1_{PNC}) = Q_W k_{PNC}/N$, where k_{PNC} is a quantity that can be computed from the atomic wavefunctions.

The experiment determines the ratio of $E1_{PNC}$ to a Stark mixing matrix element $Im(E1_{PNC})/\beta$, where β is the vector transition polarizability. In 1997, the most precise result to date utilizing Cesium was measured (57): $Im(E1_{PNC})/\beta = 1.5935(56)$ mV/cm. The value of Q_W is obtained from

$$Q_W = \left(\frac{E1_{PNC}/\beta}{M_{hf}/\beta} \right) \left(\frac{NM_{hf}}{k_{PNC}} \right) \quad (22)$$

where β and k_{PNC} were determined from atomic theory. In 1999, a more precise value of Q_W was extracted (58) based on two improvements: M_{hf}/β was measured and β was obtained from a precise calculation of M_{hf} . Second, the theoretical error in k_{PNC} was evaluated by benchmarking the calculation with other measurable quantities, such as hyperfine levels. With the improved data, $k_{PNC} = 0.9065(36) \times 10^{-11} e a_0$ was obtained. The new analysis gave the result $Q_W = -72.06$ (28)_{expt} (34)_{theor} that differed from the SM prediction by 2.3σ .

Over the past decade, several theoretical developments appeared to resolve the discrepancy with the SM (such as the inclusion of additional QED corrections and the Breit correction). The most detailed new corrections emerged from a new, high-precision calculation (59) that used the coupled cluster approximation and

included triple excitations in addition to the single and double excitations that were treated in earlier calculations. The result was $k_{PNC} = 0.8906(26) \times 10^{-11} e a_0$, which led to $Q_W(\text{Cs})^{\text{exp}} = -73.16(28)(20)$ in excellent agreement with the SM expectation. However, a recent reevaluation (47) of some of the contributions has changed the result to $k_{PNC} = 0.8977(40) \times 10^{-11} e a_0$ which is more consistent with earlier work (60). This leads to $Q_W = -72.58(43)$ and a value for $\sin^2 \theta_W$ quoted in Eqn. 20 of Sec. 1, when compared to the latest theoretical prediction, including a small Pauli blocking correction (61). Indeed, one expects, including updated electroweak corrections, $Q_W(\text{Cs})^{\text{SM}} = -73.24(5)$, a difference of 1.5σ from experiment. As discussed in Sec. 4, the result nevertheless continues to significantly constrain new TeV-scale lepton-quark interactions, complementing direct collider searches.

2.2 SLAC E158

After parity violation in neutral currents was observed by the SLAC E122 experiment as discussed in Sec. 1, the possibility was considered of measuring parity violation in electron-electron (Møller) scattering. The value of A_{PV} in Møller scattering is proportional to $Q_W^e G_F Q^2$ (62) and is highly suppressed. Firstly, the electron's weak charge $Q_W^e \approx -1 + 4 \sin^2 \theta_W$ is very small. Further, while sufficient luminosity can be generated by utilizing a very dense target, Q^2 for high energy electrons scattering off electrons of mass m_e in a fixed target is $\sim m_e E_{\text{beam}}$ and also very small. While Q^2 can be increased by several orders of magnitude in collider mode, it is difficult to compensate for the larger loss in luminosity.

A feasible design concept was conceived (63) after the upgrade of the SLAC linac enabled high intensity delivery of 48 GeV beam for the SLAC Linear Col-

lider. That allowed the first successful Møller A_{PV} measurement by the E158 experiment (48). However, even with a nearly 50 GeV beam, the predicted value of A_{PV} is only about 100 parts per billion (ppb) and many technical developments were required in the production and monitoring of the highly polarized electron beam, in a high luminosity target, a novel spectrometer and detection techniques. We now elaborate on the basic experimental technique for measuring A_{PV} in fixed target polarized electron scattering, setting the stage for the description of future initiatives using the same technique in Sec. 3.

The experiment was performed with 45 or 48 GeV polarized electrons in 100 ns bunches at a rate of 120 Hz. All electrons scattered from a 1.5 m long hydrogen target with angles between 4.4 and 7.5 mrad and energies between 13 and 24 GeV were focused onto a copper and quartz fiber calorimeter by a quadrupole spectrometer. The helicity of the beam was reversed from pulse to pulse in a pseudo-random pattern by using a Pockel's cell to reverse the helicity of the laser which produced the polarized electrons by photoemission from a strained GaAs crystal. The electron beam polarization was extracted via dedicated calibration runs measuring Møller scattering from a thin magnetized foil.

Care was taken to eliminate false asymmetries due, for example, to differences in beam properties correlated with helicity. The position, angle and energy of the beam were monitored with nanometer sensitivity and small corrections were made based on regular calibrations. In addition, the asymmetry was reversed every few runs by inserting a half-wave plate into the laser beam. Finally, the helicity of the beam was opposite for each of the two energies due to a $g - 2$ flip in the magnets in the beam switchyard; hence the data were collected with roughly equal statistics at the two different beam energies (45 and 48 GeV).

The asymmetry had the same magnitude and the correct sign for each of the four running configurations (half-wave plate state and beam energy), giving confidence in the results and suppressing a wide variety of possible small spurious effects.

The result of the experiment was $A_{PV} = -131 \pm 14$ (stat) ± 10 (sys) ppb. The tree-level prediction for A_{PV} at the specific experimental kinematics of E158 is about 250 ppb; the measured result demonstrated the running of $\sin^2 \theta_W$ unambiguously (more than 6σ) for the first time. The 3% shift in the running of $\sin^2 \theta_W$ to low Q noted in Sec. 1.3 results (50) in a shift in $Q_W^e = -1 + 4 \sin^2 \theta_W$ of about 40%. Care was taken to include full electroweak radiative corrections, including hard bremsstrahlung in the kinematic coverage (64), yielding the value of $\sin^2 \theta_W$ quoted in Eqn. 21, which stands currently as the best measurement at $Q^2 \ll M_Z^2$. To extract a value for Q_W^e , it is first necessary to define it unambiguously; see Sec. 5 for a full discussion. A logical choice, similar to the case of atomic parity violation discussed earlier, is to define Q_W^e in the static limit E and $Q^2 \rightarrow 0$. From the E158 result, the extracted value is $Q_W^e = -0.0369(52)$. In Sec. 4, the resulting limits on four-electron contact interactions and its complementarity to similar limits from lepton colliders will be discussed.

2.3 NuTeV

The NuTeV experiment carried out the most precise measurement of neutrino neutral current scattering utilizing neutrino beams of high energy and purity produced from the 800 GeV proton beam at Fermilab. The weak mixing angle $\sin^2 \theta_W$ was determined by measuring the ratios of neutral to charged current cross sections in deep inelastic scattering for both neutrinos (R_ν) and antineutrinos ($R_{\bar{\nu}}$) (49). By using the ratios of cross sections, a major experimental

uncertainty, the details of the composition of the neutrino beams, is largely canceled. The events were detected in an 18 m long steel-scintillator calorimeter followed by an iron-toroid spectrometer. Because the target is approximately isoscalar, the parton distribution functions (pdf's) largely cancel in the ratio, reducing theoretical uncertainties.

One potential source of theoretical uncertainty for extracting $\sin^2 \theta_W$ is the production of charm quarks via charged current interactions with strange sea quarks. The pdf $s(\xi)$, where $\xi = x(1 + m_c^2/Q^2)$ is a slow rescaling variable, must be used for the charged current whereas $s(x)$ is used for the neutral current. However, by treating both R_ν and $R_{\bar{\nu}}$ as functions of m_c and $\sin^2 \theta_W$, and combining both measurements, the m_c error can be reduced. In the simplest approximation, a linear combination of R_ν and $R_{\bar{\nu}}$ can be found that is independent of m_c and is proportional to $1 - 2 \sin^2 \theta_W$, the Paschos-Wolfenstein relation (65).

The published NuTeV result is nearly 3σ away from the SM prediction, though some small shifts in either direction are expected from updates to the K_{e3} branching ratio, radiative corrections and isospin-breaking effects. A number of phenomenological approaches exploring physics beyond the SM have been investigated to interpret the discrepancy; for a review, see for example Ref. (66).

A number of papers have been published trying to explain the NuTeV result within the context of the SM. One example invokes an asymmetric quark sea, parton-level charge symmetry violation (CSV), and a modification of light quark pdf's in the nuclear medium (so-called isovector EMC effect) to bring the experiment into perfect agreement with the SM (67). Other possibilities include radiative corrections (68) and nuclear shadowing (69, 70). Such corrections have not been incorporated formally into a reanalysis of the NuTeV result because of

concerns about the estimated theoretical uncertainties of various corrections. If CSV and the isovector EMC effect are indeed as large as given in Ref (67), it would be a significant discovery regarding fundamental QCD effects in nuclei. One of the auxiliary measurements in the proposed SoLID experiment, discussed in the next section, would provide independent confirmation of this effect.

3 PARITY-VIOLATING ELECTRON SCATTERING

In the following section, we describe the current experimental program of parity-violating electron scattering experiments. They are centered at two laboratories: the Thomas Jefferson National Accelerator Facility in Newport News, VA (JLab), and at the Institut für Kernphysik at the University of Mainz, Germany. All the experiments described here make use of and build on the experimental techniques developed and improved over the decades since the pioneering SLAC E122 experiment; an overview was provided in Sec. 2.3 in the description of SLAC E158.

The Continuous Electron Accelerator Facility (CEBAF) at JLab has been operating since 1995 with a wide dynamic range in beam energy (from 1 to 6 GeV), beam current (few nA to 180 μ A), longitudinal beam polarization ($> 85\%$) and beam stability. In 2014, an energy upgrade will be completed which will increase the maximum available beam energy to 12 GeV, with the capability of delivering 11 GeV at very high luminosity to existing experimental halls, significantly expanding the physics program (71). The Qweak experiment recently completed data collection using a 1 GeV beam energy and two new initiatives known as MOLLER and SoLID have been proposed to utilize the 11 GeV beam.

The Mainz Energy-recovering Superconducting Accelerator (MESA) is a new machine which has been approved for funding at Mainz, offering 100 MeV in

energy recovery operation and 150-200 MeV for conventional external beam mode (72). The latter mode is the one that will be used for the proposed P2 experiment. It is envisioned that first beam will be available by the end of 2017.

3.1 Qweak

The Qweak experiment (73) was designed to measure the proton's weak charge $Q_W^p \approx 1 - 4 \sin^2 \theta_W$ via A_{PV} in elastic electron-proton scattering. The experiment was first proposed in 2001, constructed between 2006 and 2009, and data collection was completed in 2012 in two run periods lasting about 11 months in total. Data analysis is ongoing and final results are expected by 2014.

The experimental design centered around achieving $\delta(A_{PV}) \approx \pm 2.1\%$ (stat.) and $\pm 1.3\%$ (syst.), resulting in $\delta(Q_W^p) \approx \pm 4\%$, and $\delta(\sin^2 \theta_W) \approx \pm 0.3\%$. The incident beam energy was 1.165 GeV. Elastically scattered electrons in the range $\theta_{lab} = 8 \pm 2^\circ \rightarrow \langle Q^2 \rangle = 0.026 \text{ GeV}^2$ were selected. The theoretical prediction at this Q^2 is $A_{PV} \approx -230$ ppb, the piece proportional to $Q_W^p G_F$ is -150 ppb and the statistical goal was $\delta(A_{PV}) \approx \pm 6$ ppb.

In Hall C at JLab, a 1 GeV 87% longitudinally polarized electron beam, with a current of $150 - 180 \mu\text{A}$, was incident on a 35 cm liquid hydrogen target capable of withstanding a heat load of 2.5 kW. Elastically scattered electrons were focused by the spectrometer/collimator system on to an azimuthally symmetric (with respect to the beam axis) arrangement of quartz bar integrating Cherenkov detectors. The electron beam helicity was reversed in a quartet pattern at 960 Hz: a helicity state was chosen pseudo-randomly at 240 Hz and 4 consecutive pulses in $(+ - - +)$ pattern or its complement were chosen accordingly. The width of the raw asymmetry distribution is a crucial bench mark; for Qweak, this width

was 230 ppm for a quartet. The contribution from counting statistics was about 200 ppm. The dominant sources of additional fluctuations were from detector resolution, target density fluctuations and beam current monitor resolution.

Methods similar to those developed for SLAC E158 (Sec. 2.3) were employed to reduce the sensitivity of the measured asymmetry to helicity-correlated beam fluctuations. Also, a new method for reversing the relative direction between the spin and momentum vectors of the incident electrons before acceleration (so-called Double Wien filter) was employed every few weeks to gain further suppression. In addition to using Møller polarimetry every few days, Qweak used a Compton polarimeter that monitored the electron beam polarization continuously, concomitant with physics data collection; it is anticipated that the absolute beam polarization will be known to better than 1%. The absolute value of $\langle Q^2 \rangle$ was calibrated in separate low current runs using special purpose drift-chambers that could track individual scattered electrons.

3.2 MOLLER

The MOLLER experiment (74) is a new initiative proposed to measure A_{PV} in Møller scattering a factor of 5 better than the E158 result. As was pointed out in Sec. 2.2, $A_{PV} \propto Q_W^e \approx -1 + 4 \sin^2 \theta_W$ which is reduced from its tree-level value by $\sim 40\%$ due to radiative corrections. This reduces the sensitivity of the extracted value of $\sin^2 \theta_W$ to normalization errors such as beam polarization by an additional factor of two compared to A_{PV} in elastic electron-proton scattering. The goal is a 2.3% measurement of Q_W^e resulting in $\delta(\sin^2 \theta_W)_{\text{stat}} \approx 0.00025$, $\mathcal{O}(\pm 0.1\%)$, similar to the two best high energy collider extractions of the parameter from measurements of Z^0 decays (see Sec. 1).

The MOLLER design shares many similarities with E158 and Qweak. An 11 GeV electron beam in JLab Hall A will be incident on a 1.5 meter LH_2 target. A toroidal spectrometer would exploit the unique topology of Møller scattering involving identical particles, avoiding the typical 50% azimuthal acceptance loss associated with coil placement. This is accomplished by employing an odd number of coils and collecting scattered electrons from both the forward and backward directions in the center of mass frame. The Møller-scattered electrons in the full range of the azimuth would be directed to a ring focus 30 m downstream of the target. The detector system would incorporate a great deal of redundancy to monitor the principal backgrounds from electron-proton elastic and inelastic scattering to better than 1% accuracy. The prediction for A_{PV} is 35.6 ppb and the statistical error goal is 0.74 ppb.

MOLLER will greatly benefit from the steady improvement in the techniques employed to measure parity-violating asymmetries to sub-ppb systematic precision and to also achieve normalization control at the sub-% level. For example, two redundant continuous monitors of electron beam polarization would be employed to achieve 0.4% fractional accuracy. Auxiliary detectors would track individual particles at low rates to measure $\langle Q^2 \rangle$ to 0.5% fractional accuracy. Very forward angle detectors downstream of the main detectors would verify that luminosity fluctuations due to jitter in electron beam properties and target density are under control. All three methods to reverse the sign of the asymmetry that have been developed for previous experiments ($g - 2$ spin flip, half-wave plate insertion and the double Wien filter) would also be employed periodically. Technical design efforts for MOLLER are ongoing and it is envisioned that funding approval will be obtained in 2013 so that construction of the apparatus could be

gin in 2015 which would allow commissioning by 2017, soon after full luminosity beams become available at Jefferson Laboratory.

3.3 Deep Inelastic Scattering at 6 GeV

The first measurement of A_{PV} in deep-inelastic scattering since the original SLAC E122 measurement discussed in Sec. 1.1 (20) was carried out by JLab experiment E08011 (75). The primary motivation was to measure the poorly known neutral current axial-vector quark couplings. The experiment ran in late 2009 with an incident beam energy of ~ 6 GeV and $Q^2 \sim 1 - 2$ GeV², collecting sufficient statistics to measure A_{PV} off ²H with a fractional accuracy better than 4%.

The scattered electrons were detected by the Hall A High Resolution Spectrometer (HRS) pair (76). Unlike other high rate experiments discussed in this review, a custom fast counting data acquisition system was used. Event-by-event particle identification was carried out at the hardware level with gas Cherenkov detectors and lead-glass shower counters. This information was fed into fast trigger logic to form electron and pion triggers that were in turn fed into scalers. The electron scaler results over the duration of each helicity time window of the electron beam were used to construct the raw asymmetry from which A_{PV} could be extracted. The electron trigger efficiency was found to be greater than 95%, with a pion rejection $> 1000 : 1$. Data analysis is ongoing and final results are expected to be published by late 2013.

3.4 SOLID

The SoLID experiment (77) at JLab has been proposed to make a series of A_{PV} measurements with 0.5–1% fractional accuracy in deep inelastic scattering of

electrons off ^2H . The primary motivation is to measure new linear combinations of vector and axial-vector quark couplings with sufficient accuracy to provide new and complementary access to new TeV-scale lepton-quark interactions. It would also result in a measurement of $\sin^2 \theta_W$ with an uncertainty of $\delta(\sin^2 \theta_W) \approx 0.0006$ at $Q \sim 2.5$ GeV.

The heart of the apparatus is a large acceptance solenoid such as one of several that have been used over the past couple of decades to provide the magnetic field inside collider detectors. This facilitates A_{PV} measurements in narrow x_{bj} , Q^2 bins: $0.3 \lesssim x_{bj} \lesssim 0.7$, with a lever arm of a factor of 2 in Q^2 while keeping $W_{\min}^2 > 4$ GeV 2 and $\langle Q^2 \rangle \sim 5$ GeV 2 . Such a large volume and high field solenoid is required to achieve sufficient statistics at the highest possible Q^2 and x_{bj} , provided at least 50% azimuthal acceptance is obtained. It facilitates shielding the detectors from target photons and sweeping out low energy charged particles, while accommodating a significant target length and large laboratory scattering angles. The LD $_2$ target would be placed inside the solenoidal field and several planes of absorbing material between the target and detectors with slits would tailor the momentum acceptance to the kinematic region interest.

One important feature is that, unlike other A_{PV} measurements that integrate detector signals over different helicity periods, high precision hit-based tracking with gas electron multiplier detectors is required to reconstruct the scattering angle and momentum of scattered electrons. To separate electrons from background, predominantly a 100 times more π^- particles, particle identification would be performed with heavy-gas Cerenkov detectors placed symmetrically about the beam axis inside the solenoid. An electromagnetic calorimeter would provide the primary electron trigger as well as allow additional pion rejection.

A proposal for the experiment was approved in January 2010 at JLab and detailed simulations have been carried out for the case of using the solenoid from the CLEO-II detector in the CESR e^+e^- storage ring. A significant R&D program has been launched to develop a detailed experimental design and the project will seek funding over the next few years to run at JLab.

3.5 P2

The P2 experiment has been proposed for the newly funded MESA facility at Mainz. The goal is $\delta(A_{PV}) = \pm 1.7\%$ (stat. + syst.) for elastic electron-proton, which would yield $\delta(Q_W^p) \simeq 2\%$ and $\delta(\sin^2 \theta_W) \pm 0.15\%$. To achieve the statistics would require a 200 MeV, 150 μA beam incident on a 60 cm LH_2 target for 10,000 hours. Apart from the improvement in statistical reach and hence sensitivity to new physics over the JLab Qweak experiment, the lower beam energy reduces theoretical uncertainties in extracting $\sin^2 \theta_W$ (see Sec. 5.3).

The design requires a solenoidal magnet (such as the inner tracking field of the ZEUS collider detector at DESY) downstream of the target which would focus scattered electrons within $10^\circ < \theta_{\text{lab}} < 30^\circ$ in the full range of the azimuth onto integrating Cherenkov detectors. The field would sweep out the large Møller electron background and allow judiciously placed annular slits to shield the detectors from the target's direct photon background. The theoretical prediction is $A_{PV} \sim 20$ ppb and $\delta(A_{PV})(\text{stat.})$ is ± 0.25 ppb. The total rate in the detectors would approach 0.5 THz.

The design must overcome many technical challenges such as controlling electron beam fluctuations at the sub-nm level and controlling target density fluctuations to a few parts in 10^{-5} . A new method to measure the electron beam

polarization must be developed, which would require a novel polarized hydrogen gas target (78). The design and required R&D will be carried out in the next few years so that the experiment would be ready to start commissioning when MESA first produces external beams, anticipated for 2017.

4 SENSITIVITY TO PHYSICS BEYOND THE STANDARD MODEL

We now discuss the sensitivity of precision low Q^2 measurements of weak neutral current amplitudes to physics beyond the SM. We choose a few specific topics; many comprehensive reviews (79, 29) have studied aspects of the sensitivity to supersymmetric (80, 56) as well as non-supersymmetric (81) new physics.

4.1 New Contact Interactions

If there is new physics beyond the SM at some scale Λ above the electroweak scale, then in measurements at $Q^2 \ll \Lambda^2$ new dynamics can manifest themselves as small deviations from the expected SM rates. The new dynamics appear as contact interaction terms in an effective Lagrangian (82) that interfere with SM amplitudes. They can be parametrized as:

$$\mathcal{L}_{\text{eff}} = \frac{g^2}{(1 + \delta)\Lambda^2} \sum_{i,j=L,R} \eta_{ij}^f \bar{e}_i \gamma_\mu e_i \bar{f}_j \gamma^\mu f_j, \quad (23)$$

summed over helicities ($\delta = 0(1)$ for $f = e(f \neq e)$). A typical convention sets $g^2/(4\pi) = 1$ and the $\eta_{ij}^f = \pm 1$ or 0. Precision measurements can then be translated into bounds on Λ . The effective Lagrangian in Eq.(23) can be induced by a range of new physics scenarios such as low scale quantum gravity with large extra dimensions, composite fermions, leptoquarks, heavy Z' bosons etc.

One can classify models that induce contact interactions according to the choices for the η_{ij}^f ; a representative sample (83) is shown in Table 1. The superscripts (+, -) indicate constructive and destructive interference with the SM respectively. Searches for such new contact interactions have been carried out in electron-positron, electron-proton, and hadron colliders.

The LL^\pm model, shown in Table 1, is a benchmark scenario commonly used in contact interaction searches. For the $eeqq$ -type contact interactions, assuming quark flavor independence, sensitive limits come from analyses of cross-sections and asymmetries at LEP (84, 85): $\Lambda^- > 8.0$ TeV and $\Lambda^+ > 9.7$ TeV (95% C.L.). Similarly, $\Lambda^- > 7.0$ TeV and $\Lambda^+ > 4.5$ TeV were obtained for $eeee$ -type contact interactions. More comprehensive bounds for several of the other models in Table 1 can be found in Ref. (86). More recently, the ATLAS (87) collaboration derived bounds on the LL^\pm model via measurements of fully-inclusive Drell-Yan production in the dielectron channel, obtaining $\Lambda^- > 9.5$ TeV, $\Lambda^+ > 12.1$ TeV for the LL^\pm $eeqq$ -type contact interaction.

Low Q^2 weak neutral current measurements discussed in Secs. 2 and 3 can also probe contact interactions competitive with colliders. Specifically, the parity violation measurements are sensitive to contact interactions of the form

$$\begin{aligned} \mathcal{L} = & -\frac{G_F}{\sqrt{2}} \sum_q \left[C_{1q} \bar{e} \gamma^\mu \gamma_5 e \bar{q} \gamma_\mu q + C_{2q} \bar{e} \gamma^\mu e \bar{q} \gamma_\mu \gamma_5 q \right] \\ & - \frac{G_F}{\sqrt{2}} C_{2e} \bar{e} \gamma^\mu \gamma_5 e \bar{e} \gamma_\mu e, \end{aligned} \quad (24)$$

where the sum over “ q ” is over the quark flavors and the coefficients C_{1q} , C_{2q} , C_{2e} are given by the sum of SM and new contact interaction contributions. Bounds on specific couplings can be translated into bounds on Λ . For example, the E158 measurement (Sec. 2.2) can be used to extract a value of the weak charge of

the electron (in the static limit, see Sec. 5) $Q_W^e = 2C_{2e} \approx -1 + 4\sin^2\theta_W = -0.0369(52)$ compared to the SM prediction of $-0.0435(9)$. One can then extract 95% C.L. limits on Λ using

$$\Lambda \simeq \frac{2\sqrt{\pi}}{\sqrt{\sqrt{2}G_F\Delta Q_W^e}} \quad (25)$$

to obtain $\Lambda_{LL}^+ \geq 6.7$ TeV and $\Lambda_{LL}^- \geq 14.2$ TeV. Two things are worth pointing out. Firstly, the sensitivity is better than the limits from LEP, underscoring the power of measuring a small SM coupling such as $C_{2e}G_F$ to high precision. Secondly, the LEP limits come from measurements above W^+W^- threshold. The precise $\sin^2\theta_W$ measurements at the Z^0 resonance are not as sensitive to contact interactions amplitudes; the imaginary SM amplitude on top of the Z^0 resonance does not interfere with them. The proposed MOLLER measurement (Sec. 3.2) would improve these Λ limits to nearly 20 TeV, the best sensitivity to new flavor-conserving four-lepton contact interactions in existing facilities anywhere in the world. Better limits would require the construction of new facilities such as a linear collider, Z^0 factory or neutrino factories, all of which are at least a decade away from fruition.

The chiral structures for $eeqq$ -type contact interactions that appear in Eqn. 24 correspond to the AV^\pm (C_{1i}) and VA^\pm (C_{2i}) class of models in Table 1. Limits on the VA^\pm class of $eeqq$ -type contact interactions in Table 1 were obtained by the H1 (88) and Zeus (89) experiments studying electron-proton and positron-proton collisions in the deep inelastic regime to give $\Lambda^- > 3.6$ TeV, $\Lambda^+ > 3.8$ TeV and $\Lambda^- > 3.2$ TeV, $\Lambda^+ > 3.3$ TeV respectively.

A_{PV} and APV measurements in semi-leptonic reactions discussed in Sec. 2 and Sec. 3 have complementary and improved sensitivity. Over the last two decades, several experiments have measured A_{PV} in elastic electron-proton scattering at

$0.1 < Q^2 < 1 \text{ GeV}^2$ with the aim of constraining the strange quark form factors of the proton (90). Global fits to the data determined that the strange form factors were constrained to be small enough (91, 92, 93) that the low Q^2 forward angle data could then be analyzed to extract a measurement of $Q_W^p = 2(2C_{1u} + C_{1d})$. By expanding the parity-violating asymmetry at small scattering angles in powers of Q^2 with the parametrization $A_{PV} \propto Q_W^p + Q^2 B(Q^2)$, and then combining with the atomic parity violation result on Cesium discussed in Sec. 2.1 (which measures $C_{1u} + C_{1d}$), independent determinations of C_{1u} and C_{1d} were obtained (94). This led to new constraints on the AV^\pm chiral structure of $\sim 3 \text{ TeV}$ independently for $eeuu$ - and $eedd$ -type interactions, comparable to the H1 and ZEUS limits.

The Qweak measurement (Sec. 3.1) will improve the sensitivity to the specific linear combination of AV^\pm interaction $2C_{1u} + C_{1d}$ to better than 10 TeV, while the APV result on Cesium already has similar sensitivity reach for $C_{1u} + C_{1d}$. The SoLID measurement would have sensitivity to a new linear combination of VA^\pm $eeqq$ -type contact interactions at the level of 8.9 TeV. Note that improving Λ sensitivity beyond 10 TeV in a variety of chiral structures is necessary for a comprehensive search, as demonstrated by an example discussed at the end of the next section. The Λ reach and the specific coupling combinations of various experiments discussed in this review are summarized in Table 2.

4.2 New Heavy Z' Bosons

Z' bosons with mass $M_{Z'}$ in the TeV range appear in many extensions of the SM, including $SO(10)$, E_6 , Little Higgs, and extra-dimensional theories. They arise from an additional $U(1)'$ gauge group appearing in such new physics constructions. The phenomenology has been extensively reviewed (95, 96), and the

impact of precision electroweak data on a wide range of Z' models extensively analyzed (97,98). Z' 's have been constrained by electroweak precision data (97,99), interference effects at LEP-II (86), and the Tevatron (100) with limits ~ 1 TeV.

The simplest discovery mode for Z' bosons would be through an s -channel resonance in the dilepton or dijet topologies at colliders. The LHC will be able to explore the 1–5 TeV range of Z' masses, although extracting detailed properties such as the width and couplings will be difficult for $M'_Z \gtrsim 2$ TeV. In the region $M'_Z \lesssim 2$ TeV, a detailed study of the couplings will be enhanced by an analysis of off-peak LHC data and low-energy electroweak precision data. In such analyses, where the interaction energies are well below the Z' mass ($M_{Z'}$), its exchange can be described by contact interactions where $\Lambda \sim M_{Z'}$. Constraints on contact interactions can then be translated into bounds on the mass and couplings of the Z' boson. For example, for Z' exchange between electrons and quarks, with the LL^\pm chiral structure of Table 1, $M_{Z'}^2/(g_e^L g_q^L) \simeq \Lambda^2/(4\pi^2)$ where g_e^L, g_q^L are the left-handed Z' couplings to electrons and quarks respectively.

Low Q^2 A_{PV} measurements can be quite sensitive to Z' bosons due to their sensitivity to the interference between the electromagnetic amplitude and the Z' contact interaction. Further, they probe different chiral combinations of Z' couplings compared to the LHC, helping remove degeneracies in parameter space in a purely LHC data-based analysis (101). In the context of exploring the reach of low energy experiments, a class of E_6 based Z' -models was recently analyzed (102). Such Z' models arise from the spontaneous symmetry breaking chain $E_6 \rightarrow SO(10) \times U(1)_\psi \rightarrow SU(5) \times U(1)_\chi \times U(1)_\psi \rightarrow \text{SM} \times U(1)'$. The Z' associated with the remaining $U(1)'$ can be written in general form

$$Z' = \cos \alpha \cos \beta Z_\chi + \sin \alpha \cos \beta Z_Y + \sin \beta Z_\psi, \quad (26)$$

where $Z_{\chi, Y, \psi}$ are gauge bosons associated with $U(1)_{\chi, Y, \psi}$ in the gauge eigenstate basis, β is the mixing angle between $U(1)_{\chi}$ and $U(1)_{\psi}$, and the angle α is non-vanishing in the presence of kinetic mixing between the $U(1)'$ and $U(1)_Y$ gauge groups. The angles α and β in Eq.(26) provide a way to parameterize the class of E_6 based models. For example, the Z_{χ}, Z_{ψ} , and Z_{η} models correspond to $\alpha = 0$ and $\beta = 0^0, 90^0, -\arctan\sqrt{5/3}$ respectively. An example of how low energy results and future initiatives discussed in this review complement collider searches is demonstrated in Fig. 1 of Ref. (102), which shows excluded regions in the (α, β) parameter space for a hypothetical $M'_Z = 1.2$ TeV.

One particularly unique sensitivity of low Q^2 A_{PV} measurements is with that to the so-called lepto-phobic Z' boson that only couples to quarks and is thus difficult to discover at hadron colliders due to the irreducible QCD backgrounds. As mentioned in the previous section, measurements of the C_{2i} couplings by the proposed SOLID experiment (Sec. 3.4) will provide new sensitivity to $VA^{\pm} eeqq$ -type contact interactions. Recently, it has been pointed out (103, 104) that these couplings can be modified by a $\gamma - Z'$ vacuum-polarization one-loop correction, thus extending the current < 100 GeV reach to 150 – 200 GeV.

4.3 Dark Parity Violation

Some recent new physics scenarios have relatively light new degrees of freedom and hence cannot be classified in terms of contact interactions. The failure to observe such scenarios in high energy experiments implies that such light particles must couple very weakly to SM particles. In certain regions of parameter space, low energy precision experiments can have unique or enhanced sensitivity. In this context, the possibility of a “dark” Z boson (105, 106), denoted as Z_d and of mass

m_{Z_d} , stemming from a spontaneously broken $U(1)_d$ gauge symmetry associated with a secluded “dark” particle sector was recently investigated. The Z_d boson can couple to the SM through a combination of kinetic and mass mixing with photon and the Z^0 -boson, with couplings ε and $\varepsilon_Z = \frac{m_{Z_d}}{m_Z} \delta$ respectively.

The original scenario with kinetic mixing with the photon was conjectured (107, 108, 109, 110) to explain astrophysical observables as well as to account for the long standing deviation of the muon’s anomalous magnetic moment, a_μ , from SM expectations (111). Taking into account various experimental constraints, the a_μ discrepancy is naturally accommodated by kinetic mixing in the range

$$|\varepsilon| \simeq 2 \times 10^{-3} \quad 20 \text{ MeV} \lesssim m_{Z_d} \lesssim 50 \text{ MeV}. \quad (27)$$

In the presence of mass mixing ($\delta \neq 0$), a new source of “dark” parity violation arises (105) such that it has negligible effect at the Z^0 pole precision data, but is quite discernable at low Q^2 through a shift in the weak mixing angle (106):

$$\Delta \sin^2 \theta_W(Q^2) \simeq -0.42 \varepsilon \delta \frac{m_Z}{m_{Z_d}} \left(\frac{m_{Z_d}^2}{Q^2 + m_{Z_d}^2} \right). \quad (28)$$

In this scenario, the small (1.5σ) APV deviation, $\Delta \sin^2 \theta_W(0) \simeq -0.003(2)$ suggests $\delta \simeq \pm 1 - 4 \times 10^{-3}$ as a potentially interesting region that can be explored by future APV or A_{PV} measurements, as we elaborate in the next section.

4.4 Weak Charges and New Physics

Employing the very precisely measured values of α , G_F , and m_Z along with m_t and $m_H = 126 \text{ GeV}$ in the one-loop corrected SM, but allowing for very heavy new particle loop effects via the electroweak precision S and T parameters (112, 45) leads to the predictions

$$m_W = 80.362(6) \text{ GeV} [1 - 0.0036 S + 0.0056 T],$$

$$\sin^2 \theta_W(m_Z)_{\overline{MS}} = 0.23124(6)[1 + 0.0157S - 0.0112 T]. \quad (29)$$

Comparison with experiment currently yields $S = 0.07 \pm 0.09$ and $T = 0.10 \pm 0.09$ which can be used to significantly constrain models such as Technicolor or the properties of 4th generation fermions.

Similarly, the weak charges of particles and nuclei (defined at the static limit, E and $Q^2 \rightarrow 0$) are precisely predicted at the loop level (26). However, in addition to S and T , deviations can be induced by new physics in other ways. For example, Z' gauge bosons can cause $\mathcal{O}(m_Z^2/m_{Z'}^2)$ shifts in the weak charges similar to that seen in Eqn. (25) for generic contact interactions.

To illustrate relative sensitivities, we consider the Z_χ model of $SO(10)$ that violates parity in a well-specified manner (45, 113). Also, to allow new physics differences between $\sin^2 \theta_W(m_Z)_{\overline{MS}}$ and $\sin^2 \theta_W(0)_{\overline{MS}}$ beyond SM running effects, we introduce $X(Q^2)$ (114, 50), which is similar to S , but Q^2 -dependent. For heavy particle loops (eg. SUSY or heavy fermions (115)) with a generic mass scale M where $X(Q^2) \sim \mathcal{O}(\alpha Q^2/M^2)$, X is already well constrained by the bounds on S from W and Z measurements. However, for very light new physics like the MeV-scale “dark” boson (Sec. 4.3), Z_d , that mixes with γ and Z^0 , thus providing a new source of dark parity violation (105, 106), $X(Q^2) \propto m_{Z_d}^2/(Q^2 + m_{Z_d}^2)$ terms can occur that are only visible in low $Q^2 \lesssim m_{Z_d}^2$ experiments.

Given these new physics scenarios, one finds the following shifts in the weak charges (45, 50, 61)

$$\begin{aligned} Q_W^e &= -0.0435(9)[1 + 0.25 T - 0.34 S + 0.7 X(Q^2) + 7m_Z^2/m_{Z_\chi}^2], \\ Q_W^p &= 0.0707(9)[1 + 0.15 T - 0.21 S + 0.43 X(Q^2) + 4.3m_Z^2/m_{Z_\chi}^2], \\ Q_W^{(12C)} &= -5.510(5)[1 - 0.003 T + 0.016 S - 0.033 X(Q^2) - m_Z^2/m_{Z_\chi}^2], \end{aligned}$$

$$Q_W(^{133}\text{Cs}) = -73.24(5)[1 + 0.011 S - 0.023 X(Q^2) - 0.9m_Z^2/m_{Z_\chi}^2], \quad (30)$$

where the uncertainties have been somewhat expanded to account for as yet uncalculated higher order effects. Several interesting features are apparent. The large $\sim 40\%$ radiative corrections to Q_W^e improve its fractional sensitivity to new physics relative to Q_W^p . That makes Møller scattering better from a systematic (such as polarization) perspective, but statistically similar in difficulty: $\delta(Q_W^e) \sim \pm 2\%$ is roughly equivalent to $\delta(Q_W^p) \sim \pm 1\%$. Both cases probe S and T below ± 0.1 and $m_{Z_\chi} \sim 2$ TeV.

For nuclei such as ^{12}C or ^{133}Cs , the T -dependence is small (45). Assuming $|S| \lesssim 0.1$ (based on existing constraints) suggests that they should be viewed as having mainly Z' and $X(Q^2)$ sensitivity. In the case of Z_χ , a $\pm 0.3\%$ measurement of $Q_W(^{12}\text{C})$ or $Q_W(^{133}\text{Cs})$ is roughly equivalent to $\delta(Q_W^e) \sim \pm 2\%$.

For $X(Q^2)$ effects such as due to low mass Z_d particles (105, 106, 109, 116) with $m_{Z_d} \sim 20 - 50$ MeV discussed in the previous section, APV experiments where Q^2 is naturally small ($Q^2 \ll m_{Z_d}^2$) are superior probes because they do not have the $m_{Z_d}^2/(Q^2 + m_{Z_d}^2)$ suppression. However, Q_W^e and Q_W^p are fractionally far more sensitive to $X(Q^2)$. For example, the $-0.9 \pm 0.6\%$ shift in the APV Cs result would lead to a 27% shift in Q_W^e if measured at the same Q . For $m_{Z_d} \sim 50$ MeV, the proposed MOLLER measurement ($Q \sim 75$ MeV) would see an 8.4% shift ($\sim 3.7\sigma$). We later show that polarized eC scattering may also be a good probe of parity violating Z_d effects if low $\langle Q \rangle$ can be achieved.

5 SELECTED THEORETICAL ISSUES

5.1 Radiative Corrections to Parity-Violating Møller Scattering

The asymmetry A_{PV} in the Møller scattering process $e^-e^- \rightarrow e^-e^-$ (62) is a powerful probe of new physics with relatively small theoretical uncertainties. In the mid-1990's, the proposed precision of the E158 measurement (Sec. 2.2) spurred the calculation of one-loop corrections, which shifts A_{PV} for Møller scattering by about 40% (50). Indeed, given the plans to further improve on the E158 measurement (the MOLLER proposal, Sec. 3.2), significant progress has been made to control uncertainties in A_{PV} from higher-order radiative corrections at better than the 1% level (50, 117, 118, 53, 119, 120). For $Q^2 \ll m_Z^2$, the tree level expression is modified by radiative corrections as follows (50):

$$\begin{aligned}
 A_{PV} &= -\frac{\rho G_F Q^2}{\sqrt{2}\pi\alpha} \frac{1-y}{1+y^4+(1-y)^4} \{1 - 4\kappa(0) \sin^2 \theta_W(m_Z)_{\overline{\text{MS}}}\} \\
 &+ \frac{\alpha(m_Z)}{4\pi\hat{s}^2} - \frac{3\alpha(m_Z)}{32\pi\hat{s}^2\hat{c}^2} (1-4\hat{s}^2)[1+(1-4\hat{s}^2)^2] \\
 &+ F_1(y, Q^2) + F_2(y, Q^2) \}, \tag{31}
 \end{aligned}$$

where $y = Q^2/s$, \sqrt{s} is the center of mass energy, $\hat{s} \equiv \sin \theta_W(m_Z)_{\overline{\text{MS}}}$, and $\hat{c} \equiv \cos \theta_W(m_Z)_{\overline{\text{MS}}}$. The overall factor of $\rho = 1 + \mathcal{O}(\alpha)$ arises from radiative corrections (31, 50) to G_F , which is defined through the muon decay process. The two terms in the second line of Eqn (31) arise from WW and ZZ box diagram contributions respectively. The WW box correction gives a $\sim 4\%$ enhancement to the asymmetry. The ZZ box contribution, however, is suppressed by $(1 - 4\sin^2 \theta_W)$ and gives only a $\sim 0.1\%$ correction. The $F_1(y, Q^2)$ term (50) includes box, external leg, and vertex corrections involving at least one photon. The dominant effect, however, arises from the $\gamma - Z^0$ vacuum polarization and anapole moment contributions (see Fig. 2) that are encoded in $\kappa(0)$. The effective

weak mixing angle at $Q^2 = 0$ in terms of the $\overline{\text{MS}}$ value at the Z^0 pole is defined in terms of $\kappa(0)$ as

$$\sin^2 \theta_W(0) = \kappa(0) \sin^2 \theta_W(m_Z)_{\overline{\text{MS}}}, \quad (32)$$

corresponding to Eq.(21) evaluated at $Q^2 = 0$. However, the experiment is conducted at finite Q^2 and the corresponding finite- Q^2 vacuum polarization effects are contained in $F_2(y, Q^2)$ which is very small (50).

A purely perturbative one-loop calculation gives

$$\begin{aligned} \kappa(0) = & 1 - \frac{\alpha}{2\pi\hat{s}^2} \left\{ \frac{1}{3} \sum_f (T_{3f}Q_f - 2\hat{s}^2Q_f^2) \ln \frac{m_f^2}{m_Z^2} \right. \\ & \left. - \left(\frac{7}{2}\hat{c}^2 + \frac{1}{12} \right) \ln \hat{c}^2 + \left(\frac{7}{9} - \frac{\hat{s}^2}{3} \right) \right\}, \end{aligned} \quad (33)$$

where the sum in the first line is over the quark and lepton flavors. However, it is known that at $Q^2 = 0$ the light quark contribution to the $\gamma - Z^0$ vacuum polarization is non-perturbative and must be estimated using a dispersion relation that relates these effects to data on $e^+e^- \rightarrow \text{hadrons}$. The result of such an analysis (121,36,50) leads to the replacement (for the quark contribution)

$$\frac{1}{3} \sum_f (T_{3f}Q_f - 2\hat{s}^2Q_f^2) \ln \frac{m_f^2}{m_Z^2} \rightarrow -6.88 \pm 0.06 \quad (34)$$

in Eqn. (33), where the error in Eqn. 34 has been updated by the analysis presented in Ref. (53), which we discuss in detail in the next section. It is these hadronic vacuum polarization effects that are primarily responsible for the large $\sim 40\%$ NLO correction to the asymmetry. Coupled with anapole moment effects, they lead to the effective weak mixing angle $\sin^2 \theta_W(0)$ in Eq.(32) to differ from $\sin^2 \theta_W(m_Z)_{\overline{\text{MS}}}$ by 3%, referred to as the ‘‘running’’ from $Q^2 \sim m_Z^2$ to $Q^2 \ll m_Z^2$.

After accounting for the one-loop effects discussed above, one can now define the electron’s weak charge Q_W^e in the limit E and $Q^2 \rightarrow 0$ as a static property

of the electron, with the value quoted in Eqn. 30 for $m_H = 126$ GeV. Efforts are underway (122,123) towards completing the full next-to-next-to-leading order (NNLO) calculation of electroweak radiative corrections to the asymmetry, which are expected to shift Q_W^e possibly at the 1–2% level. Such efforts are essential in the context of the ultra-precise MOLLER proposal.

5.2 Running of the Weak Mixing Angle

An analysis similar to the one presented above must be carried out for any weak neutral current experiment that aims to measure $\sin^2 \theta_W$ better than 1% at $Q^2 \ll m_Z^2$; careful consideration must be given to the dynamics that lead to the running of $\sin^2 \theta_W$. In general, perturbative corrections enhanced by large logarithms of $\sim m_Z^2/Q^2$ (or m_Z^2/m_f^2 , where m_f is some light fermion mass) can significantly affect a reliable interpretation of low Q^2 measurements. For example, the $\sim 40\%$ reduction in the weak charge of the electron Q_W^e , and thus A_{PV} in Møller scattering (50), is due to the replacement (as discussed in Secs. 1.3, 2.2 and 5.1)

$$1 - 4 \sin^2 \theta_W(m_Z)_{\overline{\text{MS}}} \rightarrow 1 - 4\kappa(0) \sin^2 \theta_W(m_Z)_{\overline{\text{MS}}}. \quad (35)$$

$\kappa(0)$ encodes the radiative corrections from $\gamma - Z^0$ mixing and some anapole moment effects, motivating the definition of an effective weak mixing angle

$$\sin^2 \theta_W(0) \equiv \kappa(0) \sin^2 \theta_W(m_Z)_{\overline{\text{MS}}}, \quad (36)$$

which simply corresponds to Eq.(21) evaluated at $Q^2 = 0$. The quantity $\sin^2 \theta_W(0)$ incorporates a set of universal radiative corrections that also affect other low energy measurements such as APV and Qweak. The perturbative one loop result (50) for $\kappa(0)$ was given in Eqn. 33 and non-perturbative effects are incorporated by the replacement in Eqn. 34. Note that the one loop result for $\kappa(0)$ contains

large logarithms of m_Z^2/m_f^2 (at finite Q^2 there will also be large logarithms of m_Z^2/Q^2) that can spoil convergence. Higher precision extractions of $\sin^2 \theta_W$ at low Q^2 require a resummation of such large logarithms, bringing the theory under better control and facilitating a more precise interpretation of measurements.

A well-known way to incorporate resummation of large logarithms is to work in the $\overline{\text{MS}}$ -scheme for $\sin^2 \theta_W$ as defined in Eqn. 8. It uses a well-defined gauge independent subtraction scheme to remove divergent terms arising in calculations of quantum corrections that use dimensional regularization. This subtraction scheme induces a logarithmic dependence on the renormalization scale μ which is governed by a renormalization group (RG) equation. Choosing $\mu^2 \sim Q^2$ of the process avoids the appearance of large logarithms in m_Z^2/Q^2 . The $\overline{\text{MS}}$ scheme also employs threshold matching to avoid large logarithms in m_Z^2/m_f^2 when $\mu \gg m_f$ or $\mu \ll m_f$. Crossing the particle mass threshold from above, the corresponding particle is integrated out and the running below continues within an effective theory without this particle. These threshold matchings manifest themselves as discontinuities in the weak mixing angle running.

In the $\overline{\text{MS}}$ scheme, the quantity of interest for low energy experiments is $\sin^2 \theta_W(0)_{\overline{\text{MS}}}$ corresponding $\mu = 0$ in Eqn. 8. It is defined in terms of the Z^0 -pole value of the weak mixing angle as $\sin^2 \theta_W(0)_{\overline{\text{MS}}} = \kappa(0)_{\overline{\text{MS}}} \sin^2 \theta_W(m_Z)_{\overline{\text{MS}}}$, where the quantity $\kappa(0)_{\overline{\text{MS}}}$ is obtained by solving the renormalization group equation between $\mu = m_Z$ and $\mu = 0$. More generally,

$$\sin^2 \theta_W(Q^2)_{\overline{\text{MS}}} = \kappa(Q^2, \mu)_{\overline{\text{MS}}} \sin^2 \theta_W(\mu^2)_{\overline{\text{MS}}}, \quad (37)$$

gives the relation between the weak mixing angle at some fixed Q^2 in terms of its value at an arbitrary scale μ . Note that the product $\kappa(Q^2, \mu)_{\overline{\text{MS}}} \sin^2 \theta_W(\mu^2)_{\overline{\text{MS}}}$ in Eqn. 37 is independent of the scale μ . This allows one to choose $\mu^2 = Q^2$

(along with threshold matching), effectively moving large logs from $\kappa(Q^2, \mu)_{\overline{\text{MS}}}$ into $\sin^2 \theta_W(\mu^2)_{\overline{\text{MS}}}$ so that resummation can be performed using the RG evolution equation of $\sin^2 \theta_W$. On the other hand, choosing $\mu^2 = m_Z^2$ introduces large logarithms of Q^2/m_Z^2 in $\kappa_{\overline{\text{MS}}}(Q^2, \mu = m_Z)$ spoiling the convergence of perturbation theory. In Ref. (53), a solution to the RG equation of $\sin^2 \theta_W(\mu)_{\overline{\text{MS}}}$, for evolution between scales μ_0 and μ without crossing any particle mass thresholds, was given to be

$$\begin{aligned} \sin^2 \theta_W(\mu)_{\overline{\text{MS}}} &= \frac{\alpha(\mu)_{\overline{\text{MS}}}}{\alpha(\mu_0)_{\overline{\text{MS}}}} \sin^2 \theta_W(\mu_0)_{\overline{\text{MS}}} + \lambda_1 \left[1 - \frac{\alpha(\mu)}{\alpha(\mu_0)} \right] \\ &+ \frac{\alpha(\mu)}{\pi} \left[\frac{\lambda_2}{3} \ln \frac{\mu^2}{\mu_0^2} + \frac{3\lambda_3}{4} \ln \frac{\alpha(\mu)_{\overline{\text{MS}}}}{\alpha(\mu_0)_{\overline{\text{MS}}}} + \tilde{\sigma}(\mu_0) - \tilde{\sigma}(\mu) \right]. \end{aligned} \quad (38)$$

In the above equation, $\lambda_{1,2,3}$ are numerical coefficients that take on different values depending on the range (μ_0, μ) . This solution resums leading logs $\mathcal{O}(\alpha^n \ln^n \frac{\mu}{\mu_0})$, next-to-leading logs $\mathcal{O}(\alpha^{n+1} \ln^n \frac{\mu}{\mu_0})$ and $\mathcal{O}(\alpha \alpha_s^n \ln^n \frac{\mu}{\mu_0})$, next-to-next-to-leading logs $\mathcal{O}(\alpha \alpha_s^{n+1} \ln^n \frac{\mu}{\mu_0})$, and next-to-next-to-next-leading logs $\mathcal{O}(\alpha \alpha_s^{n+1} \ln^n \frac{\mu}{\mu_0})$. Non-perturbative effects arise from the contribution of light quark loops in self-energy $\gamma - Z^0$ mixing diagrams when $\mu \sim \Lambda_{QCD}$. These non-perturbative effects are incorporated in Eqn. 38 through the non-perturbative effects in the evolution of $\alpha(\mu)_{\overline{\text{MS}}}$ and in the $\tilde{\sigma}(\mu_0), \tilde{\sigma}(\mu)$ terms. These non-perturbative effects contribute an uncertainty in the extraction of $\sin^2 \theta_W(0)_{\overline{\text{MS}}}$ below the 10^{-4} level.

The value of $\sin^2 \theta(0)_{\overline{\text{MS}}}$, in terms of $\sin^2(m_Z)_{\overline{\text{MS}}}$, can be obtained by using Eqn. 38 combined with threshold matchings to evolve between the scales $\mu = m_Z$ and $\mu = 0$. It was shown in Ref. (53) that the solution to the $\overline{\text{MS}}$ RG evolution, expanded to one-loop order is

$$\kappa(0)_{\overline{\text{MS}}} = \kappa(0) + \frac{2\alpha(m_Z)}{9\pi\hat{s}^2} = \kappa(0)^{PT} = 1.03232 \pm 0.00029, \quad (39)$$

where non-perturbative effects have been included. The uncertainty has been

improved by an order of magnitude compared to previous estimates. The quantity $\kappa(0)^{PT}$ (54), is related to $\kappa(0)$ by the inclusion of additional so-called “pinch-parts” of one-loop vertex and box graphs to make it process-independent and intrinsically gauge-invariant. In the $\overline{\text{MS}}$ scheme, these additional pinch terms arise (53) from threshold matching corrections at $\mu = m_W$. Thus, working in the $\overline{\text{MS}}$ scheme allows one to reproduce the known one-loop result while allowing for the inclusion of the leading higher order corrections through resummation.

In Fig. 1, we show the running of $\sin^2 \theta_W(Q^2)$ and $\sin^2 \theta_W(Q^2)_{\overline{\text{MS}}}$ for comparison. Based on the work described above and the prediction for $\sin^2 \theta_W$ discussed Sec. 1 using fundamental SM input parameters including m_H , we obtain:

$$\sin^2 \theta_W(m_Z)_{\overline{\text{MS}}} = 0.23124(6) \rightarrow \sin^2 \theta_W(0)_{\overline{\text{MS}}} = 0.23871(9). \quad (40)$$

5.3 Weak Charge of the Proton

One can extract Q_W^p from the measurement of A_{PV} in electron-proton scattering. However, that requires considerations beyond the perturbative approach used for Møller scattering (Sec. 5.1). In particular, one must address hadronic physics that induces an energy dependence (124) to the $\gamma - Z^0$ box diagram (Fig. 3). A definition of the weak charge that isolates such effects is (125)

$$A_{PV} = -\frac{G_F Q^2}{4\sqrt{2}\pi\alpha} \frac{W^{PV}}{W^{EM}}, \quad Q_W^p = \lim_{Q^2 \rightarrow 0} \frac{W^{PV}}{W^{EM}} \Big|_{E=0}, \quad (41)$$

where we have written the asymmetry in terms of the general response functions W^{EM}, W^{PV} which depend on the electromagnetic and weak nucleon form factors. The conditions $E = 0, Q^2 = 0$ in the definition of Q_W^p , ensure that Q_W^p can be interpreted as a static property of the proton, independent of kinematics.

The tree-level SM value of $Q_W^p = 2(2C_{1u} + C_{1d}) = 1 - 4\sin^2 \theta_W$, corresponding to the sum of the weak charges of the valence quarks in the proton, receives cor-

rections from perturbative radiative effects and non-perturbative hadronic effects.

The asymmetry A_{PV} can be written as

$$A_{PV} = -\frac{G_F Q^2}{4\sqrt{2}\pi\alpha} \left[\rho_{ep}(1 - 4\sin^2\theta_W(0)_{\overline{MS}}) + \text{Re } \square_{WW} + \text{Re } \square_{ZZ} + \text{Re } \square_{\gamma Z} \right] - \frac{G_F Q^2}{4\sqrt{2}\pi\alpha} B(Q^2), \quad (42)$$

where $\rho_{ep} = 1 + \mathcal{O}(\alpha)$ radiative corrections (absorbing universal and process-dependent terms explicitly defined in Eqn. 12 of Ref. (125)) due to the normalization of the weak neutral current ep amplitude relative to the charged current muon decay amplitude used to define G_F , and \square_{WW} , \square_{ZZ} , and $\square_{\gamma Z}$ are contributions from the two-boson box graphs in Fig. (3). The remaining contribution $B(Q^2)$ parametrizes proton structure at low Q^2 and vanishes in the forward limit ($B(Q^2) \rightarrow 0$ as $Q^2 \rightarrow 0$). Comparing Eqns. 41–42 gives

$$Q_W^p = \left[\rho_{ep}(1 - 4\sin^2\theta_W(0)_{\overline{MS}}) + \text{Re } \square_{WW} + \text{Re } \square_{ZZ} + \text{Re } \square_{\gamma Z} \right] \Big|_{E=0, Q^2 \rightarrow 0}. \quad (43)$$

All the box graphs appearing in Eqn (42) are ultraviolet finite. The \square_{WW} and \square_{ZZ} box graphs (26,121,126) give perturbative corrections of $\sim 26\%$ and $\sim 3\%$ to Q_W^p respectively, independent of the electron energy since loop momenta of order M_Z dominate. Remarkably, these corrections nearly cancel the reduction in Q_W^p due to the effect of $\kappa(0)$ (Eqn. 37), which makes it seem like Q_W^p does not run with Q^2 , in stark contrast to Q_W^e .

The calculation of the $\square_{\gamma Z}$ contribution is more complicated since it is sensitive to small momentum scales and non-perturbative long distance physics. Pinning down the size of the correction and theoretical uncertainty of the $\square_{\gamma Z}$ contribution has been the subject of active research for almost three decades and continues

even today. This contribution can be written as the sum of two terms

$$\square_{\gamma Z} = \square_{\gamma Z_A} + \square_{\gamma Z_V}, \quad (44)$$

corresponding to the Z^0 -electron axial-vector (g_A^e) and vector (g_V^e) coupling contributions respectively. The first calculation of $\square_{\gamma Z}$ was carried out (121, 26) in the context of atomic parity violation where the electron energy $E \approx 0$. A cancellation between the box and crossed box graphs leads to a negligible contribution from $\square_{\gamma Z_A}$. The second and dominant contribution is

$$\text{Re } \square_{\gamma Z_V} = \frac{5\alpha(m_Z)_{\overline{\text{MS}}}}{2\pi} g_V^e \left[\ln \frac{m_Z^2}{\Lambda^2} + C_{\gamma Z}(\Lambda) \right] \quad (45)$$

suppressed by the weak vector coupling of the electron $g_V^e = 1 - 4 \sin^2 \theta_W(m_Z)_{\overline{\text{MS}}}$. In Eqn. 45, $\Lambda \sim 1$ GeV, is a hadronic cutoff that separates the perturbative and non-perturbative contributions. The first term arises from a perturbative contribution from loop momenta greater than Λ and the second term is the remaining non-perturbative contribution estimated to be $C_{\gamma Z}(\Lambda) = 3/2 \pm 1$ for $\Lambda = m_\rho$. This estimate was based on the Born approximation where the elastic proton intermediate state dominates the hadronic effects. The perturbative contribution in Eqn. 45 was recomputed (53, 126, 127), confirming the original result.

Recently, the $\square_{\gamma Z}$ contribution was reexamined in the context of the kinematics of the Qweak experiment. It was shown (124) that there is a contribution, not considered in previous analyses, that grows with the incident electron energy. In the forward limit $Q^2 \rightarrow 0$, a dispersion relation relates the real and imaginary parts of the $\square_{\gamma Z}$ contribution as

$$\begin{aligned} \text{Re } \square_{\gamma Z_A}(E) &= \frac{2E}{\pi} \int_{\nu_\pi}^{\infty} \frac{d\nu'}{\nu'^2 - E^2} \text{Im } \square_{\gamma Z_A}(\nu'), \\ \text{Re } \square_{\gamma Z_V}(E) &= \frac{2}{\pi} \int_{\nu_\pi}^{\infty} \frac{\nu' d\nu'}{\nu'^2 - E^2} \text{Im } \square_{\gamma Z_V}(\nu'), \end{aligned} \quad (46)$$

and the imaginary parts are given in terms of the PVDIS $\gamma - Z$ interference structure functions $F_{1,2,3}^{\gamma Z}(x, Q^2)$ as (124, 128, 129, 125)

$$\begin{aligned} \frac{\text{Im } \square_{\gamma Z_A}}{\alpha g_A^e} &= \int_{W_\pi^2}^s \frac{dW^2}{(s - M^2)^2} \int_0^{Q_{\text{max}}^2} \frac{dQ^2}{1 + \frac{Q^2}{M_Z^2}} \left[F_1^{\gamma Z} + \frac{s(Q_{\text{max}}^2 - Q^2)}{Q^2(W^2 - M^2 + Q^2)} F_2^{\gamma Z} \right] \\ \frac{\text{Im } \square_{\gamma Z_V}}{-\alpha g_V^e} &= \int_{W_\pi^2}^s \frac{dW^2}{(s - M^2)^2} \int_0^{Q_{\text{max}}^2} \frac{dQ^2}{1 + \frac{Q^2}{M_Z^2}} \left[\frac{2(s - M^2)}{W^2 - M^2 + Q^2} - 1 \right] F_3^{\gamma Z} \quad (47) \end{aligned}$$

where $x = Q^2/(2p \cdot q)$, $W^2 = (p + q)^2$, $W_\pi^2 = (M + \pi)^2$, $\nu_\pi = (W_\pi^2 - M^2)/(2M)$, $Q_{\text{max}}^2 = (s - M^2)(s - W^2)/s$, and p is the initial proton momentum. The explicit overall factor of the electron energy E in $\text{Re } \square_{\gamma Z_A}$, seen in Eqn. 46, is the origin of the new electron energy dependence in $\square_{\gamma Z}$. Note that while the $\square_{\gamma Z_V}$ contribution is suppressed by g_V^e , no such suppression exists for $\square_{\gamma Z_A}$, resulting in a significant energy-dependent correction to the Qweak asymmetry.

As seen in Eqns. 46–47, estimating the size of the $\square_{\gamma Z}$ contribution requires knowledge of the $F_{1,2,3}^{\gamma Z}$ structure functions over a wide range of kinematics. This range can be classified into three regions: (i) elastic ($W^2 = M^2$), (ii) resonance ($W_\pi^2 \leq W^2 \lesssim 4\text{GeV}^2$), and (iii) deep inelastic ($W^2 > 4\text{GeV}^2$). Note that since $Q^2 = 0.026\text{GeV}^2$ in Qweak, the structure functions cannot be expressed in terms of the leading twist pdfs as is usually done when $Q^2 \gg \Lambda_{QCD}^2$. A combination of data and modeling of the structure functions is necessary in the three regions for an accurate estimate of $\square_{\gamma Z}$. Moreover, the dispersion relations in Eqn. 46 were derived in the forward limit, leading to an additional Q^2 dependence in the box graphs mentioned above which was found (125) to be small.

There have been several recent estimates (124, 128, 129, 125, 130) of the size of the $\square_{\gamma Z}$ contribution and its associated uncertainty in determining Q_W^p . While this is still an active area of research with some differences between approaches and results, the general consensus is that $\square_{\gamma Z}$ contributes a $\sim 5 - 6\%$ correc-

tion for $E_{beam} \sim 1$ GeV that must be subtracted to determine Q_W^p as defined in Eqn. 43, with a $\sim 2 - 3\%$ uncertainty; the anticipated experimental uncertainty is 4%. The larger of the uncertainty estimates has a contribution from model dependence associated with flavor rotations. Auxiliary measurements from current and future JLab experiments discussed in this review will cover a wider range of $F_{1,2,3}^{\gamma Z}$ and further reduce the theoretical uncertainty in $\square_{\gamma Z_A}$. The theoretical uncertainty is already negligible for the P2 proposal (Sec. 3.5), with $E_{beam} \sim 0.2$ GeV.

6 OTHER POTENTIAL FUTURE MEASUREMENTS

6.1 Atomic Parity Violation

A number of new APV projects are underway. Two separate initiatives are being pursued on heavier atoms to take advantage of the greatly enhanced parity-violating amplitudes at higher values of Z . At TRIUMF in Canada, an experiment is under design to use Fr (131) atoms while at KVI in the Netherlands, Ra^+ ions (132) are being investigated. In both designs, chains of isotopes could potentially be measured, such that the atomic theory uncertainties cancel when ratios of different isotopes are taken. However, it must be pointed out that the measurement of Q_W for a single isotope, properly normalized to the atomic theory, will remain important since it has rather different sensitivities to new physics effects. Indeed, there are often scenarios where new physics effects also tend to cancel when isotope ratios are taken. There are also plans to measure isotope chains in Dy and Yb (133), though the atomic theory is more challenging. These measurements will also be sensitive to the thickness of the radius of the neutron distribution, which is a subject of considerable interest in itself (134).

6.2 Neutrino Scattering

Currently, the NuTeV deep-inelastic neutrino scattering result (Eqn. 20) represents the best neutrino determination of the weak mixing angle ($\sim \pm 0.7\%$). It differs by nearly 3σ from SM expectations; a situation that requires resolution. The advent of future high intensity neutrino sources, designed primarily for neutrino oscillation studies, could in principle resolve the NuTeV anomaly. For example, a fine-grained near-detector at the Fermilab LBNE facility has been suggested as a means of achieving $\pm 0.2\%$ sensitivity at Q^2 values similar to NuTeV (135).

Low energy neutrino sources such as nuclear power reactors, spallation neutron sources, β -beams etc used in conjunction with very massive detectors would be capable of measuring $\sin^2 \theta_W(m_Z)_{\overline{\text{MS}}}$ at very low $\langle Q \rangle \sim 1 - 30$ MeV using ν_e and ν_μ scattering on electrons. Fractional sensitivities of $\sim \pm 1\%$ on $\sin^2 \theta_W$ appear feasible. Unfortunately, to reach the $\pm 0.1\%$ goal appears very challenging both statistically and systematically. Nevertheless, it is a well-motivated goal, since at that level they probe many interesting varieties of “new physics” (136, 137, 138, 139, 140).

6.3 Parity Violating Electron Scattering off ^{12}C

More than two decades ago, a measurement (141) in $\bar{e}-^{12}\text{C}$ elastic scattering of $A_{PV}(eC) \propto G_F Q^2 \sin^2 \theta_W$ at the MIT-Bates laboratory achieved $\pm 25\%$ precision. Along the way, techniques were developed that set the stage for parity-violating electron scattering experiments of the type discussed in this review.

Today, higher electron currents with better longitudinal polarization combined with a much larger acceptance spectrometer (142) could potentially improve the statistical figure of merit by 10^4 , making an asymmetry measurement of $Q_W(^{12}\text{C})$

to about $\pm 0.3\%$ statistically feasible. While controlling the sources of spurious false asymmetries at the level required have been developed and are similar to those of other proposed A_{PV} measurements, controlling normalization errors and in particular the measurement of the electron beam polarization will require a detailed study. Assuming a total $\pm 0.3\%$ determination of $Q_W(^{12}\text{C})$ is possible, what can we learn, compared to other A_{PV} measurements, from such an effort?

Referring to the discussion in Sec. 4.4 and Eqn. 30 in particular, we already pointed out that in terms of m_{Z_χ} sensitivity, a $\pm 0.3\%$ measurement of $Q_W(^{12}\text{C})$ is roughly equivalent to the future MOLLER proposal to determine $Q_W(e)$ to $\pm 2.3\%$. It also represents about a factor of 3 improvement over $Q_W(\text{Cs})$ where a 1.5σ difference between theory and experiment currently exists.

Perhaps another compelling motivation for a new ultra-precise $Q_W(^{12}\text{C})$ measurement comes from the sensitivity to a light Z_d dark gauge boson (105, 106) introduced in Sec. 4.3. Indeed, explaining the $(g-2)_\mu$ 3.6σ discrepancy with $20 \text{ MeV} \lesssim m_{Z_d} \lesssim 50 \text{ MeV}$ and $\epsilon \approx 2 \times 10^{-3}$ γ - Z_d mixing, as well as accommodating the 1.5σ discrepancy in $Q_W(\text{Cs})$ requires an $X(Q^2)$ corresponding to

$$\Delta \sin^2 \theta_W(Q^2) \approx -0.003(2) \frac{m_{Z_d}^2}{Q^2 + m_{Z_d}^2} \quad (48)$$

which is to be compared with a ± 0.0007 experimental sensitivity of a $\pm 0.3\%$ $A_{PV}(^{12}\text{C})$ measurement.

At the Mainz-MESA facility, the measurement might be feasible using the same concept as that for the P2 proposal (Sec. 3.5). With the projected technical capabilities for other proposed A_{PV} initiatives, a series of three simultaneous $\pm 0.3\%$ measurements with $100 \lesssim Q \lesssim 150 \text{ MeV}$ at $E_{\text{beam}} \sim 200 \text{ MeV}$ and a second series of $\pm 0.4\%$ measurements with $60 \lesssim Q \lesssim 100 \text{ MeV}$ at $E_{\text{beam}} \sim 140 \text{ MeV}$ could be contemplated. While the statistics would be achievable in two 1-

year runs, the systematic control of normalization errors merits a detailed study.

Getting to a lower Q than 60 MeV would be challenging without new experimental technologies. Nevertheless, a program of measurements could become quite compelling depending on the results of ongoing A_{PV} and dark matter initiatives, or if the 50–100 MeV mass range for Z_d becomes important to explore. Together, a factor of 3 overall improvement compared to the existing Cs APV measurement, and the low Q^2 sensitivity to $X(Q^2)$ and “dark Z_d ” effects may be enough to motivate a new, much higher sensitivity $A_{PV}(^{12}\text{C})$ program.

6.4 Weak Mixing Angle at an Electron-Ion Collider

The design of a new experimental facility known as the Electron Ion Collider (EIC) is under study as the next logical step in the study of QCD in nuclear matter (143). One operational mode will involve high energy collisions of highly polarized electrons with polarized ^1H , ^2H and ^3He with $20 \lesssim \sqrt{s} \lesssim 150$ GeV and luminosity $\sim 10^{33-34} \text{cm}^2\text{s}^{-1}$. The collider environment and the envisioned hermetic detector package at high luminosity will allow precision A_{PV} measurements over a wide kinematic range with little uncertainty from limited knowledge of pdfs and negligible impact of higher-twist effects.

By mapping A_{PV} as a function of Q^2 and the fractional energy loss of the scattered electron y (something that is very challenging to do in fixed target experiments), a clean separation of two linear combination of couplings namely $2C_{1u} - C_{1d}$ and $2C_{2u} - C_{2d}$ will become feasible as a function of Q^2 . Thus, at the highest luminosities and center-of-mass energies envisioned at the EIC, very precise measurements of these combinations can be achieved at a series of Q^2 values, allowing a series of precision $\sin^2 \theta_W$ extractions. Figure 4 shows the projected

uncertainties on the weak mixing angle extracted from such a dataset (144), for a center of mass energy of 140 GeV and an integrated luminosity of 200 fb^{-1} .

7 SUMMARY AND OUTLOOK

Precision measurements of electroweak parameters have played an important role in confirming the SM and probing for “new physics” effects. The recent (tentative) discovery of the Higgs boson at the LHC, with $m_H \approx 126 \text{ GeV}$ completes the elementary particle spectrum of the minimal SM and allows even more refined predictions and comparisons between theory and experiment.

Already, determinations of m_W and $\sin^2 \theta_W(m_Z)_{\overline{\text{MS}}}$ (at the Z^0 pole) test SM expectations at better than $\pm 0.1\%$ and find no glaring evidence for discrepancies (although m_W is somewhat high and $\sin^2 \theta_W(m_Z)_{\overline{\text{MS}}}$ measurements have a broader spread than one would like). Those tests confirm the SM at its quantum loop level and constrain “new physics” appendages to it; examples include fourth generation fermions, technicolor, supersymmetry, GUTs etc.

Low Q^2 SM observables, such as weak neutral current charges Q_W , can also be precisely computed and compared with measurements. Results from classic measurements such as Cs APV and SLAC E158 are currently at about the $\pm 0.5\text{--}1\%$ sensitivity for $\sin^2 \theta_W(Q^2 \approx 0)$. At that level, they test quantum loops and confirm the anticipated running of $\sin^2 \theta_W(Q^2)$ by about 3% as it evolves from $Q^2 \approx 0$ to m_Z^2 . In addition, those measurements play a special role in constraining Z' , leptoquark models, and generic 4-fermion contact interactions.

There is rich physics in the radiative corrections that leads for example to the remarkable numerical difference between the electron and the proton renormalized weak charges. This has implications for the design, feasibility and systematic

error propagation for precision experiments. The difference also serves to emphasize the value of studying the SM with high precision in as many reactions as possible. A priori, one cannot know where new physics may be observed; physics that can be described at low energies by new contact interactions or physics that appears in vacuum polarization or box diagrams at the quantum loop level.

Now a new generation of polarized electron scattering experiments are on the horizon. Qweak at JLab has completed data collection and is in the analysis stage. It will improve the low Q^2 determination of $\sin^2 \theta_W(Q^2)$ to $\pm 0.3\%$ with little theoretical uncertainty, given the recent advances in the evaluation of γZ^0 box diagrams. We will soon see if the result presents any surprises.

The tremendous technical advances in experimental methods as well as the theoretical advances in precision calculations have set the stage for very low Q^2 ee and ep asymmetry measurements that will aim for unprecedented $\pm 0.1\%$ $\sin^2 \theta_W(Q \approx 0)$ sensitivity, allowing them to be competitive with the best Z^0 pole studies. At that level, Z' models and contact interactions are probed at mass scales in the 1–20 TeV range, the running of $\sin^2 \theta_W(Q^2)$ is precisely verified or perhaps dramatically new phenomena are uncovered. For example, low Q^2 measurements may unveil “Dark Parity Violation” due to a very light, weakly coupled Z_d boson from the dark matter sector. If found, such a discovery would revolutionize the focus of low energy parity violation experiments and provide strong motivation for other challenging low and high energy experiments designed to shed new light on “Dark Physics”.

Surprises advance science, but they are only possible if we push the boundaries of our abilities.

Acknowledgment

We thank J. Erler, Y. Li and M. Ramsey-Musolf for useful discussion and input on figures. This work has been funded in part by the United States Department of Energy under grant contract numbers DE-FG02-88R40415-A018 (KK), DE-AC02-98CH10886 (WJM), DE-FG02-84ER40146 (PAS), and by the U.S. National Science Foundation under grant NSF-PHY- 0705682 (SM). WJM acknowledges partial support as a Fellow in the Gutenberg Research College.

LITERATURE CITED

1. Glashow S, Nucl.Phys. 22:579 (1961).
2. Weinberg S, Phys.Rev.Lett. 19:1264 (1967).
3. Higgs PW, Phys.Lett. 12:132 (1964).
4. Higgs PW, Phys.Rev.Lett. 13:508 (1964).
5. Higgs PW, Phys.Rev. 145:1156 (1966).
6. Englert F, Brout R, Phys.Rev.Lett. 13:321 (1964).
7. Guralnik G, Hagen C, Kibble T, Phys.Rev.Lett. 13:585 (1964).
8. Bouchiat C, Iliopoulos J, Meyer P, Phys.Lett. B42:91 (1972).
9. 't Hooft G, Nucl.Phys. B35:167 (1971).
10. Gargamelle Neutrino Collaboration, Hasert F, et al., Phys.Lett. B46:138 (1973).
11. Bollini C, Giambiagi J, Sirlin A, Nuovo Cim. A16:423 (1973).
12. Marciano W, Nucl.Phys. B84:132 (1975).
13. Bouchiat M, Bouchiat C, J.Phys.(France) 35:899 (1974).
14. Lewis L, Hollister J, Soreide D, Lindahl E, Fortson E, Phys.Rev.Lett. 39:795 (1977).

15. Baird P, Brimicombe S, Hunt R, Roberts G, Sandars P, et al., Phys.Rev.Lett. 39:798 (1977).
16. Barkov L, Zolotarev M, JETP Lett. 27:357 (1978).
17. Conti R, Bucksbaum P, Chu S, Commins E, Hunter L, Phys.Rev.Lett. 42:343 (1979).
18. Bucksbaum P, Commins E, Hunter L, Phys.Rev.Lett. 46:640 (1981).
19. Bouchiat M, Guena J, Hunter L, Pottier L, Phys.Lett. B117:358 (1982).
20. Prescott C, Atwood W, Cottrell RL, DeStaebler H, Garwin EL, et al., Phys.Lett. B77:347 (1978).
21. Georgi H, Glashow S, Phys.Rev.Lett. 32:438 (1974).
22. Georgi H, Quinn HR, Weinberg S, Phys.Rev.Lett. 33:451 (1974).
23. Marciano WJ, Phys.Rev. D20:274 (1979).
24. Marciano WJ, Senjanovic G, Phys.Rev. D25:3092 (1982).
25. Marciano W, Sirlin A, Phys.Rev.Lett. 46:163 (1981).
26. Marciano WJ, Sirlin A, Phys.Rev. D29:945 (1984).
27. Aoyama T, Hayakawa M, Kinoshita T, Nio M, Phys.Rev.Lett. 109:111807 (2012), 1205.5368.
28. MuLan Collaboration, Tishchenko V, et al., (2012), 1211.0960.
29. Particle Data Group, Beringer J, et al., Phys.Rev. D86:010001 (2012).
30. Sirlin A, Phys.Rev. D22:971 (1980).
31. Marciano W, Sirlin A, Phys.Rev. D22:2695 (1980).
32. Marciano W, Sirlin A, Conf.Proc. C810424:151 (1981).
33. Gambino P, Sirlin A, Phys.Rev. D49:1160 (1994), hep-ph/9309326.
34. SLD Collaboration, Abe K, et al., Phys.Rev.Lett. 84:5945 (2000), hep-ex/0004026.

35. ALEPH Collaboration, CDF Collaboration, D0 Collaboration, DELPHI Collaboration, L3 Collaboration, OPAL Collaboration, SLD Collaboration, LEP Electroweak Working Group, Tevatron Electroweak Working Group, SLD Electroweak and Heavy Flavour Groups, (2010), 1012.2367.
36. Marciano WJ, Proceedings, Spin Structure in High Energy Processes :35 (1993).
37. FerrogliA A, Ossola G, Passera M, Sirlin A, Phys.Rev. D65:113002 (2002), hep-ph/0203224.
38. Awramik M, Czakon M, Freitas A, Weiglein G, Phys.Rev. D69:053006 (2004), hep-ph/0311148.
39. Awramik M, Czakon M, Freitas A, JHEP 0611:048 (2006), hep-ph/0608099.
40. Marciano WJ, eConf C040802:L009 (2004), hep-ph/0411179.
41. Marciano WJ, p. 48 (2000), hep-ph/0003181.
42. ATLAS Collaboration, Aad G, et al., Phys.Lett. B716:1 (2012), 1207.7214.
43. CMS Collaboration, Chatrchyan S, et al., Phys.Lett. B716:30 (2012), 1207.7235.
44. FerrogliA A, Sirlin A, (2012), 1211.1864.
45. Marciano WJ, Rosner JL, Phys.Rev.Lett. 65:2963 (1990).
46. Marciano WJ, J.Phys.Conf.Ser. 312:102002 (2011).
47. Dzuba V, Berengut J, Flambaum V, Roberts B, Phys.Rev.Lett. 109:203003 (2012), 1207.5864.
48. SLAC E158, Anthony PL, et al., Phys. Rev. Lett. 95:081601 (2005), hep-ex/0504049.
49. NuTeV Collaboration, Zeller G, et al., Phys.Rev.Lett. 88:091802 (2002), hep-ex/0110059.

50. Czarnecki A, Marciano WJ, *Phys.Rev.* D53:1066 (1996), hep-ph/9507420.
51. Czarnecki A, Marciano WJ, *Int.J.Mod.Phys.* A13:2235 (1998), hep-ph/9801394.
52. Czarnecki A, Marciano WJ, *Int.J.Mod.Phys.* A15:2365 (2000), hep-ph/0003049.
53. Erler J, Ramsey-Musolf MJ, *Phys.Rev.* D72:073003 (2005), hep-ph/0409169.
54. Ferroglia A, Ossola G, Sirlin A, *Eur.Phys.J.* C34:165 (2004), hep-ph/0307200.
55. Musolf MJ, et al., *Phys. Rept.* 239:1 (1994).
56. Erler J, Su S, (2013), 1303.5522.
57. Wood C, Bennett S, Cho D, Masterson B, Roberts J, et al., *Science* 275:1759 (1997).
58. Bennett S, Wieman CE, *Phys.Rev.Lett.* 82:2484 (1999), hep-ex/9903022.
59. Porsev S, Beloy K, Derevianko A, *Phys.Rev.* D82:036008 (2010), 1006.4193.
60. Dzuba V, Flambaum V, Ginges J, *Phys.Rev.* D66:076013 (2002), hep-ph/0204134.
61. Blunden P, Melnitchouk W, Thomas A, *Phys.Rev.Lett.* 109:262301 (2012), 1208.4310.
62. Derman E, Marciano WJ, *Annals Phys.* 121:147 (1979).
63. Kumar KS, Hughes E, Holmes R, Souder P, *Mod.Phys.Lett.* A10:2979 (1995).
64. Kolomensky Y, Shumeiko N, Suarez J, Zykunov V, *Int.J.Mod.Phys.* A20:7365 (2005).
65. Paschos E, Wolfenstein L, *Phys.Rev.* D7:91 (1973).

66. Davidson S, Forte S, Gambino P, Rius N, Strumia A, JHEP 0202:037 (2002), hep-ph/0112302.
67. Bentz W, Cloet I, Londergan J, Thomas A, Phys.Lett. B693:462 (2010), 0908.3198.
68. Diener KP, Dittmaier S, Hollik W, Phys.Rev. D72:093002 (2005), hep-ph/0509084.
69. Hirai M, Kumano S, Nagai TH, Phys.Rev. D71:113007 (2005), hep-ph/0412284.
70. Brodsky SJ, Schmidt I, Yang JJ, Phys.Rev. D70:116003 (2004), hep-ph/0409279.
71. Dudek J, Ent R, Essig R, Kumar K, Meyer C, et al., Eur.Phys.J. A48:187 (2012), 1208.1244.
72. Aulenbacher K, Dehn M, Kreidel HJ, Heine R, Eichhorn R, ICFA Beam Dyn.Newslett. 58:145 (2012).
73. Armstrong D, Asaturyan A, Averett T, Benesch J, Birchall J, et al., (2012), 1202.1255.
74. MOLLER Collaboration, Mammei J, Nuovo Cim. C035N04:203 (2012), 1208.1260.
75. Jefferson Lab Hall A Collaboration, Zheng X, Nuovo Cim. C035N04:72 (2012).
76. Alcorn J, Anderson B, Aniol K, Annand J, Auerbach L, et al., Nucl.Instrum.Meth. A522:294 (2004).
77. SOLID Collaboration, Souder P, AIP Conf.Proc. 1441:123 (2012).
78. Chudakov E, Luppov V, IEEE Trans.Nucl.Sci. 51:1533 (2004).
79. Ramsey-Musolf MJ, Phys. Rev. C60:015501 (1999), hep-ph/9903264.

80. Ramsey-Musolf M, Su S, Phys.Rept. 456:1 (2008), hep-ph/0612057.
81. Chang WF, Ng JN, Wu JM, Phys.Rev. D79:055016 (2009), 0901.0613.
82. Eichten E, Lane KD, Peskin ME, Phys.Rev.Lett. 50:811 (1983).
83. Kroha H, Phys.Rev. D46:58 (1992).
84. ALEPH Collaboration, Schael S, et al., Eur.Phys.J. C49:411 (2007), hep-ex/0609051.
85. ALEPH Collaboration, DELPHI Collaboration, L3 Collaboration, OPAL Collaboration, LEP Electroweak Working Group, Schael S, et al., (2013), 1302.3415.
86. LEP Collaborations, ALEPH Collaboration, DELPHI Collaboration, L3 Collaboration, LEP Electroweak Working Group, SLD Electroweak Group, SLD Heavy Flavour Group, OPAL Collaboration, Electroweak tS, (2004), hep-ex/0412015.
87. ATLAS Collaboration, Aad G, et al., Phys. Rev. D 87, 015010 (2013), 1211.1150.
88. Aaron F, Alexa C, Andreev V, Backovic S, Baghdasaryan A, et al., Phys.Lett. B705:52 (2011), 1107.2478.
89. ZEUS Collaboration, Chekanov S, et al., Phys.Lett. B591:23 (2004), hep-ex/0401009.
90. Kumar KS, Souder P, Prog.Part.Nucl.Phys. 45:S333 (2000).
91. Young RD, Roche J, Carlini RD, Thomas AW, Phys.Rev.Lett. 97:102002 (2006), nucl-ex/0604010.
92. Liu J, McKeown RD, Ramsey-Musolf MJ, Phys.Rev. C76:025202 (2007), 0706.0226.
93. Gonzalez-Jimenez R, Caballero J, Donnelly T, (2011), 1111.6918.

94. Young RD, Carlini RD, Thomas AW, Roche J, Phys.Rev.Lett. 99:122003 (2007), 0704.2618.
95. Rizzo TG, p. 537 (2006), hep-ph/0610104.
96. Langacker P, Rev.Mod.Phys. 81:1199 (2009), 0801.1345.
97. Erler J, Langacker P, Munir S, Rojas E, JHEP 0908:017 (2009), 0906.2435.
98. Erler J, Langacker P, Munir S, Rojas E, JHEP 1111:076 (2011), 1103.2659.
99. del Aguila F, de Blas J, Perez-Victoria M, JHEP 1009:033 (2010), 1005.3998.
100. CDF Collaboration, D0 Collaboration, Jaffre M, PoS EPS-HEP2009:244 (2009), 0909.2979.
101. Li Y, Petriello F, Quackenbush S, Phys.Rev. D80:055018 (2009), 0906.4132.
102. Erler J, Langacker P, Munir S, Rojas E, (2011), 1108.0685.
103. Buckley MR, Ramsey-Musolf MJ, Phys.Lett. B712:261 (2012), 1203.1102.
104. Gonzalez-Alonso M, Ramsey-Musolf MJ, (2012), 1211.4581.
105. Davoudiasl H, Lee HS, Marciano WJ, Phys.Rev. D85:115019 (2012), 1203.2947.
106. Davoudiasl H, Lee HS, Marciano WJ, Phys.Rev.Lett. 109:031802 (2012), 1205.2709.
107. Holdom B, Phys.Lett. B166:196 (1986).
108. Fayet P, Phys.Rev. D70:023514 (2004), hep-ph/0403226.
109. Bouchiat C, Fayet P, Phys.Lett. B608:87 (2005), hep-ph/0410260.
110. Pospelov M, Phys.Rev. D80:095002 (2009), 0811.1030.
111. Muon G-2 Collaboration, Bennett G, et al., Phys.Rev. D73:072003 (2006), hep-ex/0602035.
112. Peskin ME, Takeuchi T, Phys.Rev.Lett. 65:964 (1990).
113. London D, Rosner JL, Phys.Rev. D34:1530 (1986).

114. Maksymyk I, Burgess C, London D, Phys.Rev. D50:529 (1994), hep-ph/9306267.
115. Kurylov A, Ramsey-Musolf M, Su S, Phys.Rev. D68:035008 (2003), hep-ph/0303026.
116. Davoudiasl H, Lee HS, Marciano WJ, Phys.Rev. D86:095009 (2012), 1208.2973.
117. Denner A, Pozzorini S, Eur.Phys.J. C7:185 (1999), hep-ph/9807446.
118. Petriello FJ, Phys.Rev. D67:033006 (2003), hep-ph/0210259.
119. Aleksejevs A, Barkanova S, Ilyichev A, Zykunov V, Phys.Rev. D82:093013 (2010), 1008.3355.
120. Aleksejevs A, Barkanova S, Ilyichev A, Kolomensky Y, Zykunov V, (2010), 1010.4185.
121. Marciano W, Sirlin A, Phys.Rev. D27:552 (1983).
122. Aleksejevs A, Barkanova S, Kolomensky Y, Kuraev E, Zykunov V, Phys.Rev. D85:013007 (2012), 1110.1750.
123. Aleksejevs A, Barkanova S, Bystritskiy Y, Kuraev E, Ilyichev A, et al., (2012), 1202.0378.
124. Gorchtein M, Horowitz C, Phys.Rev.Lett. 102:091806 (2009), 0811.0614.
125. Gorchtein M, Horowitz C, Ramsey-Musolf MJ, Phys.Rev. C84:015502 (2011), 1102.3910.
126. Erler J, Kurylov A, Ramsey-Musolf MJ, Phys.Rev. D68:016006 (2003), hep-ph/0302149.
127. Musolf M, Holstein BR, Phys.Lett. B242:461 (1990).
128. Sibirtsev A, Blunden P, Melnitchouk W, Thomas A, Phys.Rev. D82:013011 (2010), 1002.0740.

129. Rislow BC, Carlson CE, Phys.Rev. D83:113007 (2011), 1011.2397.
130. Blunden P, Melnitchouk W, Thomas A, Phys.Rev.Lett. 107:081801 (2011), 1102.5334.
131. Aubin S, Gomez E, Behr J, Pearson M, Sheng D, et al., AIP Conf.Proc. 1441:555 (2012).
132. Giri G, Versolato O, Wansbeek L, van den Berg J, van der Hoek D, et al., Can.J.Phys. 89:69 (2011).
133. Tsigutkin K, Dounas-Frazer D, Family A, Stalnaker J, Yashchuk V, et al., Phys.Rev.Lett. 103:071601 (2009).
134. Sil T, Centelles M, Vinas X, Piekarewicz J, Phys.Rev. C71:045502 (2005), nucl-th/0501014.
135. Mishra S, Petti R, Rosenfeld C, PoS NUFACT08:069 (2008), 0812.4527.
136. Marciano WJ, Parsa Z, J.Phys. G29:2629 (2003), hep-ph/0403168.
137. Conrad J, Link J, Shaevitz M, Phys.Rev. D71:073013 (2005), hep-ex/0403048.
138. Rosner JL, Phys.Rev. D70:037301 (2004), hep-ph/0404264.
139. de Gouvea A, Jenkins J, Phys.Rev. D74:033004 (2006), hep-ph/0603036.
140. Agarwalla SK, Huber P, JHEP 1108:059 (2011), 1005.1254.
141. Souder P, Holmes R, Kim D, Kumar KS, Schulze M, et al., Phys.Rev.Lett. 65:694 (1990).
142. Souder P, Holmes R, Pasadena 1990, Proceedings, Parity violation in electron scattering :137 (1990).
143. Deshpande A, Mezziani ZE, Qiu JW, McKeown R, Vigdor S, et al., (2012), 1212.1701.
144. Boer D, Diehl M, Milner R, Venugopalan R, Vogelsang W, et al., (2011),

1108.1713.

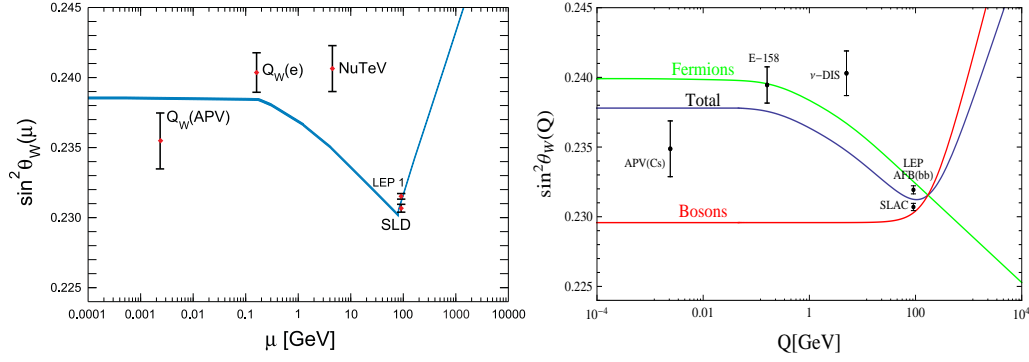


Figure 1: $\sin^2 \theta_W(\mu)_{\overline{\text{MS}}}$ (left panel) from Ref. (29) with updated APV result. $\sin^2 \theta_W(Q^2)$ (right panel), a one-loop calculation dominated by $\gamma-Z^0$ mixing (52). The red and green curves are the boson and fermion contributions respectively.

| Model | η_{LL}^f | η_{RR}^f | η_{LR}^f | η_{RL}^f |
|----------|---------------|---------------|---------------|---------------|
| LL^\pm | ± 1 | 0 | 0 | 0 |
| RR^\pm | 0 | ± 1 | 0 | 0 |
| LR^\pm | 0 | 0 | ± 1 | 0 |
| RL^\pm | 0 | 0 | 0 | ± 1 |
| VV^\pm | ± 1 | ± 1 | ± 1 | ± 1 |
| AA^\pm | ± 1 | ± 1 | ∓ 1 | ∓ 1 |
| VA^\pm | ± 1 | ∓ 1 | ± 1 | ∓ 1 |

| Experiment | Λ | Coupling |
|------------|-----------|--------------------|
| Cesium APV | 9.9 TeV | $C_{1u} + C_{1d}$ |
| E-158 | 8.5 TeV | C_{ee} |
| Qweak | 11 TeV | $2C_{1u} + C_{1d}$ |
| SoLID | 8.9 TeV | $2C_{2u} - C_{2d}$ |
| MOLLER | 19 TeV | C_{ee} |
| P2 | 16 TeV | $2C_{1u} + C_{1d}$ |

Table 2: 95% C.L. reach of experiments

Table 1: Models classified by chiral structure in the effective Lagrangian. discussed in Sec. 2 and 3 to the new physics scale Λ ($g^2 = 4\pi$)

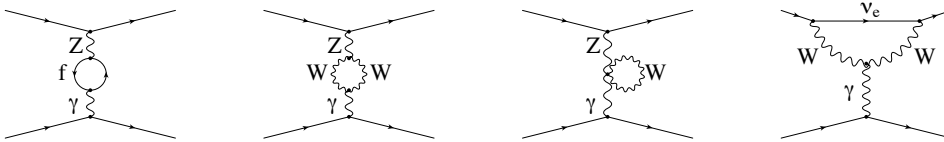


Figure 2: $\gamma-Z$ mixing diagrams and W -loop contribution to the anapole moment for parity-violating elastic electron scattering (reproduced from Ref. (52))

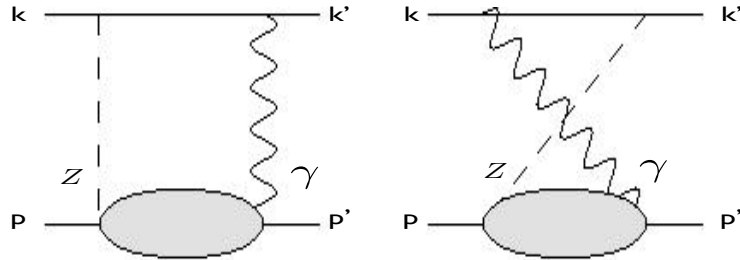


Figure 3: Box graphs contributing to $\square_{\gamma Z}$ in elastic electron-proton scattering (reproduced from Ref. (124))

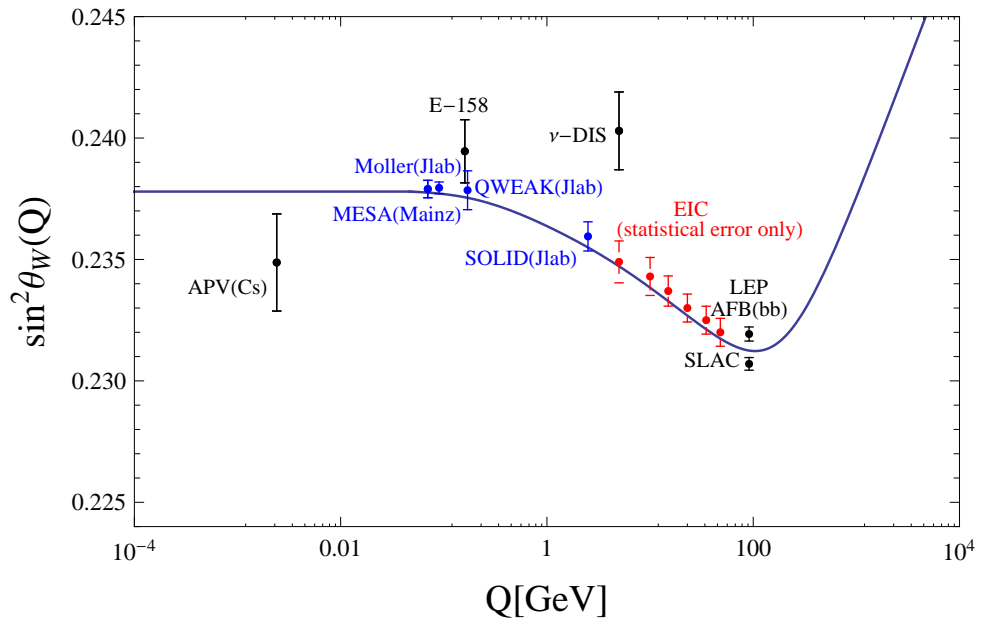


Figure 4: Current and future $\sin^2 \theta_W$ measurements. The black points are published results (Sec. 2), the blue points are projections for projects discussed in Sec. 3, and the red points are projected for the EIC, $\sqrt{s} = 140$ GeV, 200 fb^{-1} .